DEVELOPMENTAL NEUROSCIENCE

NAD$^+$-mediated rescue of prenatal forebrain angiogenesis restores postnatal behavior

Sivan Subburaju[1,2,3], Sarah Kaye[1,3], Yong Kee Choi[1,2,3], Jugajyoti Baruah[1,2,3], Debkanya Datta[1,2,3], Jun Ren[4], Ashwin Srinivasan Kumar[4,5], Gabor Szabo[6], Dai Fukumura[4], Rakesh K. Jain[4], Abdallah Elkhal[7,8], Anju Vasudevan[1,2]*

Intrinsic defects within blood vessels from the earliest developmental time points can directly contribute to psychiatric disease origin. Here, we show that nicotinamide adenine dinucleotide (NAD$^+$), administered during a critical window of prenatal development, in a mouse model with dysfunctional endothelial γ-aminobutyric acid type A ($GABA_A$) receptors (*Gabrb3* endothelial cell knockout mice), results in a synergistic repair of impaired angiogenesis and normalization of brain development, thus preventing the acquisition of abnormal behavioral symptoms. The prenatal NAD$^+$ treatment stimulated extensive cellular and molecular changes in endothelial cells and restored blood vessel formation, GABAergic neuronal development, and forebrain morphology by recruiting an alternate pathway for cellular repair, via previously unknown transcriptional mechanisms and purinergic receptor signaling. Our findings illustrate a novel and powerful role for NAD$^+$ in sculpting prenatal brain development that has profound implications for rescuing brain blood flow in a permanent and irreversible manner, with long-lasting consequences for mental health outcome.

INTRODUCTION

The global burden of neuropsychiatric disorders and their consequences has been steadily increasing, and a comprehensive understanding of risk factors in the prenatal and/or postnatal period is essential for early intervention or prevention. Our studies have established a direct autonomous link between blood vessels and the developmental roots of psychiatric disease (*1*–*5*). By investigating the importance of novel γ-aminobutyric acid (GABA)–related gene expression in embryonic forebrain endothelial cells, we selectively modulated components of the endothelial GABA signaling pathway in vivo (*1*, *5*). This approach rendered endothelial GABA type A ($GABA_A$) receptors dysfunctional and affected GABA release from endothelial cells. The disruption of autocrine and paracrine mechanisms of endothelial cell–mediated GABA signaling had far-reaching consequences for brain development, network formation, and, subsequently, for postnatal behavior (*1*, *5*). These works provided novel understanding of how endothelial cell–specific GABA and its receptor signaling shape neurovascular interactions during embryonic development and how alterations in this select pathway lead up to psychiatric disease. For instance, embryonic forebrain (telencephalic) angiogenesis was notably affected and failed to provide physical and chemoattractive guidance for long-distance migration and final distribution of GABAergic interneurons. It caused a reduction in vascular densities in the embryonic brain, which persisted in the adult brain, with morphological changes in blood vessels indicative of functional changes, accompanied by concurrent GABAergic neuronal cell deficits. This resulted in behavioral dysfunction that was characterized by impaired social recognition, reduced social interactions, communication deficits, and increased anxiety and depression and resulted in a new mouse model of psychiatric disorder—the *Gabrb3* endothelial cell knockout ($Gabrb3^{ECKO}$) mice (*1*). These findings are of high significance as they emphasize that the exclusive focus on neuropsychiatric illnesses from a neuronal perspective needs to be broadened to include intrinsic defects within the vasculature that may be the actual trigger for pathophysiological changes.

Therefore, we questioned whether we could rescue abnormal brain development by rescuing angiogenesis and neurovascular interactions in the $Gabrb3^{ECKO}$ mice, in which there are both vascular and GABAergic interneuron deficits in the prefrontal cortex (*1*). Specifically, would rescue of telencephalic angiogenesis at prenatal stages be able to restore downstream neurovascular interactions, normalize brain development, and ameliorate postnatal behavioral symptoms? A natural physiological molecule that can serve to improve cell proliferation and migration would be ideal for in vivo use, during this sensitive gestational time frame. In our previous work with nicotinamide adenine dinucleotide (NAD$^+$), a cofactor of interesting therapeutic potential, we had perceived its promising properties in promoting stem cell proliferation in the central nervous system in a multiple sclerosis model (*6*). Administration of NAD$^+$ reversed disease progression by regulating $CD4^+$ T cell differentiation and apoptosis, inducing homeostasis and promoting myelin and neuronal regeneration (*6*). As NAD$^+$ is a coenzyme found in all living cells, it is additionally able to cross the uteroplacental barrier (*7*). NADPH (reduced form of nicotinamide adenine dinucleotide phosphate) oxidase in endothelial cells has been reported to generate reactive oxygen species that stimulate angiogenic factors like vascular endothelial growth factor, with implications for postnatal angiogenesis in vivo (*8*). NAD$^+$ precursors have been used in the context of aging (*9*) and Alzheimer's disease (*10*) or to relieve postpartum metabolic stress (*11*); however, so far, there are no reports of NAD$^+$ use and impact in the prenatal developmental period.

[1]Angiogenesis and Brain Development Laboratory, Huntington Medical Research Institutes (HMRI), 686 S Fair Oaks Avenue, Pasadena, CA 91105, USA. [2]Department of Psychiatry, Harvard Medical School, Boston, MA, 02215, USA. [3]Division of Basic Neuroscience, McLean Hospital, 115 Mill Street, Belmont, MA, 02478, USA. [4]Edwin L. Steele Laboratories, Department of Radiation Oncology, Massachusetts General Hospital and Harvard Medical School, Boston, MA, 02114, USA. [5]Harvard-MIT Division of Health Sciences and Technology, Massachusetts Institute of Technology, Cambridge, MA 02139, USA. [6]Institute of Experimental Medicine, Medical Gene Technology Unit, *1*083 Budapest, Hungary. [7]Department of Surgery, Harvard Medical School, Boston, MA 02115, USA. [8]Division of Transplantation, Brigham and Women's Hospital, 221 Longwood Avenue, EBRC 309, Boston, MA 02115, USA.
*Corresponding author. Email: anju.vasudevan@hmri.org

Here, our studies highlight the importance of NAD^+ treatment during a critical window of prenatal development that can serve to rescue angiogenesis and neurovascular interactions in the embryonic telencephalon. Not only NAD^+ is beneficial for the enduring repair of nascent blood vessels but also it has a region-specific target in the embryonic telencephalon by influencing cellular and molecular mechanisms in the ganglionic eminence, a key origin site for several GABAergic interneuron populations. Our prenatal NAD^+ treatment paradigm was able to engage an alternate pathway to modulate endothelial GABA release and rescue telencephalic development in the *Gabrb3*^{ECKO} mice, leaving its lasting signatures on postnatal blood flow and behavioral outcomes. This study illustrates how prenatal forebrain angiogenesis can be instrumentalized effectively to modulate adult behaviors.

RESULTS

Prenatal NAD^+ treatment rescues angiogenesis and morphological defects in the *Gabrb3*^{ECKO} telencephalon

We first isolated periventricular endothelial cells from E15 wild-type (CD1) forebrain and tested the effect of NAD^+ addition in vitro. Exogenous addition of 100 μM NAD^+ was able to initiate significant endothelial cell proliferation within 2 days of culture, and a 35-mm culture dish was confluent within 4 to 6 days (fig. S1, A to D). This was an interesting observation since untreated periventricular endothelial cells take approximately 12 days to reach confluency in 35-mm dishes, in our well-established culture conditions (*1*, *2*, *4*, *12*). Endothelial cell bromodeoxyuridine (BrdU) labeling index was significantly increased, indicating that NAD^+ was able to robustly trigger endothelial cell proliferation (fig. S1E). Vital elements of angiogenesis include effective endothelial cell proliferation, migration, sprouting, alignment, tube formation, and branching. NAD^+-treated periventricular endothelial cells started showing tube formation properties under normal culture conditions, which was highly unusual in the absence of a substrate such as Matrigel (fig. S1, F to H). The NAD^+-treated endothelial cells demonstrated tubular network formation in the absence of a three-dimensional milieu, with budding, branching, and lumen formation (fig. S1, F to G). In some areas of the dish, the NAD^+-treated endothelial cells seemed to align and fold into tubular shapes (fig. S1H), aspects that we have not seen in wild-type or untreated periventricular endothelial cells in normal culture conditions (*1*, *2*, *4*, *12*). NAD^+-treated endothelial cells also showed robust long-distance migration, from one end of the dish to the other, in terms of cell number, when compared to untreated cells (fig. S1, I and J). Collectively, these results confirmed the high angiogenic potential of NAD^+ addition on periventricular endothelial cells. We also tested the effects of NAD^+ addition on neuronal cells isolated from the E15 CD1 forebrain and found an increase in cell proliferation (fig. S1K). NAD^+ addition similarly increased long-distance migration of neuronal cells, but the effect was more robust when neurons were seeded on periventricular endothelial cells (fig. S1L). Although the endothelial cell response to NAD^+ (fig. S1, E and J) was more pronounced than neuronal cells alone (fig. S1, K and L), these results provided convincing evidence that the NAD^+ addition was having positive effects on both cell types and formed the rationale for exploring the use of NAD^+ in vivo.

In the *Gabrb3*^{ECKO} telencephalon, labeling with multiple markers of vessel components, isolectin B4 and CD31/PECAM-1 have revealed reductions in vessel density and pattern formation from embryonic day 13 (E13) onward to E18 (*1*). This vascular deficit in the embryonic telencephalon persisted in the adult cerebral cortex with larger vessel diameters likely correlating with increased perfusion and indicative of functional changes in blood flow in *Gabrb3*^{ECKO} vessels (*1*). A summary of the embryonic and postnatal phenotype highlights (fig. S2A) the importance of the endothelial GABA pathway for telencephalic angiogenesis and for maintaining neurovascular interactions. Therefore, given its proangiogenic properties (fig. S1, A to J), we decided to test whether NAD^+ treatment during the prenatal period would be able to improve angiogenesis in the *Gabrb3*^{ECKO} telencephalon. The periventricular ventral-dorsal angiogenesis gradient is established by E11, after which neuronal cells originating from ventricular zones navigate along radial and tangential courses, to adopt final laminar positions and integrate into specific brain circuits (*2*–*4*). Therefore, our approach was to target only the critical window of mouse prenatal brain development: E12 to E17. In the *Gabrb3*^{ECKO} telencephalon, the periventricular vessel gradient is formed normally at E11, but reductions in vascular density and abnormal vascular profiles are observed from E13 onward (*1*). Hence, NAD^+ treatment (10 mg in 100 μl of saline) or a placebo solution (100 μl of saline) was given intraperitoneally daily to pregnant dams from E12 to E17 (fig. S2B). Three groups were compared throughout the study: group 1, saline-treated *Gabrb3*$^{fl/fl}$ mice or controls; group 2, saline-treated *Gabrb3*^{ECKO} mice; and group 3, NAD^+-treated *Gabrb3*^{ECKO} mice. At E18, brains were isolated and vascular densities were assessed by labeling blood vessels with biotinylated isolectin B4 in paraffin sections. A significant improvement in periventricular vessel densities was observed in NAD^+-treated *Gabrb3*^{ECKO} telencephalon versus saline-treated *Gabrb3*^{ECKO} telencephalon and was comparable to saline-treated *Gabrb3*$^{fl/fl}$ telencephalon (Fig. 1, A to D). These results implicated that the prenatal NAD^+ treatment was successful in rescuing angiogenesis in the *Gabrb3*^{ECKO} telencephalon.

Furthermore, we made another exciting finding when we examined the morphology of NAD^+-treated *Gabrb3*^{ECKO} telencephalon at E18 (Fig. 1, E1 to G5). In histological stainings, we have previously reported morphological defects in the *Gabrb3*^{ECKO} medial telencephalon at E18 along with marked ventricular abnormalities, reduced hippocampus, and enlarged striatal compartments (*1*), and these perturbations in anatomical landmarks were consistently observed in saline-treated *Gabrb3*^{ECKO} telencephalon at all rostro-caudal levels (Fig. 1, F1 to F5). Of importance, NAD^+ treatment during E12 to E17 significantly improved the overall morphology of the *Gabrb3*^{ECKO} telencephalon (Fig. 1, G1 to G5), restored anatomical landmarks and ventricular size, and was similar to saline controls (Fig. 1, E1 to E5). In the hematoxylin and eosin staining, we observed a cluster of cells in the medial ganglionic eminence (MGE) of NAD^+-treated *Gabrb3*^{ECKO} mice that were discernible specifically in the middle sections along the rostro-caudal axis. This seemed to indicate that the prenatal NAD^+ treatment had a selective target in the MGE that was quantified (Fig. 1H). Such a distinct type of cellular arrangement was not seen in other regions of the forebrain or in the midbrain and hindbrain of NAD^+-treated *Gabrb3*^{ECKO} mice. We also evaluated NAD^+-treated *Gabrb3*$^{fl/fl}$ littermates and observed the same distinct cellular arrangement in the MGE indicating that the treatment targeted the same region in all genotypes (fig. S3, A1 to A5). We next performed an increasing dose regimen of NAD^+ treatment (10, 20, and 40 mg per mouse; intraperitoneally) in wild-type CD1 mice to test whether this observation was consistent in a different strain of mice and observed a similar cell cluster in the MGE (fig. S3,

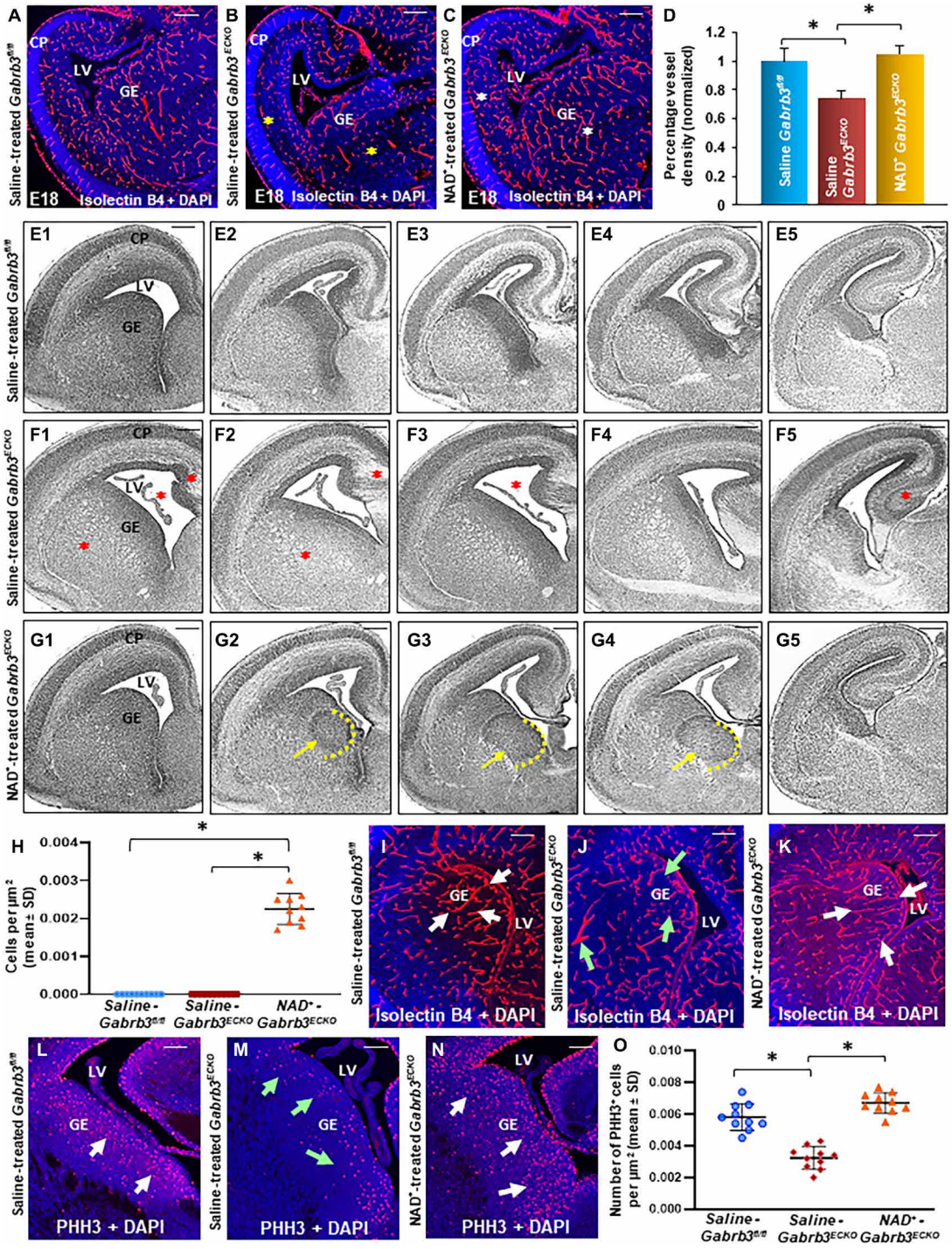

Fig. 1. NAD$^+$-mediated rescue of prenatal forebrain angiogenesis and morphological defects in the *Gabrb3^{ECKO}* telencephalon. (**A** to **C**) Fewer isolectin B4$^+$ vessels in E18 saline-treated *Gabrb3^{ECKO}* telencephalon [yellow asterisks, (B)] compared to saline-treated *Gabrb3$^{fl/fl}$* telencephalon (A) and NAD$^+$-treated *Gabrb3^{ECKO}* telencephalon [white asterisks, (C)]. DAPI, 4′,6-diamidino-2-phenylindole. (**D**) Morphometric analysis revealed significant rescue in vessel densities in NAD$^+$-treated *Gabrb3^{ECKO}* telencephalon; data represent means ± SD [$n = 10$, $^*P < 0.05$, one-way analysis of variance (ANOVA)]. (**E1** to **G5**) Hematoxylin and eosin stainings revealed morphological abnormalities in E18 saline-treated *Gabrb3^{ECKO}* telencephalon [red asterisks, (F1) to (F5)], while NAD$^+$-treated *Gabrb3^{ECKO}* telencephalon (G1 to G5) showed significant improvement in morphology, similar to saline-treated controls (E1 to E5). Yellow dotted half circles and arrows point to a NAD$^+$-mediated cellular target in the medial ganglionic eminence (MGE) (G2 to G4). (**H**) Quantification of the MGE NAD$^+$ target site ($n = 10$, $^*P < 0.0001$, one-way ANOVA). (**I** to **K**) Well-formed vascular plexus in saline-treated *Gabrb3$^{fl/fl}$* ganglionic eminence (GE) [white arrows, (I)] and NAD$^+$-treated *Gabrb3^{ECKO}* ganglionic eminence (K) that is lost in saline-treated *Gabrb3^{ECKO}* ganglionic eminence [green arrows, (J)]. (**L** to **N**) Abnormal PHH3$^+$ profiles were observed in saline-treated *Gabrb3^{ECKO}* telencephalon [green arrows, (M)] when compared to saline [white arrows, (L)] and NAD$^+$-treated *Gabrb3^{ECKO}* telencephalon (N). (**O**) Quantification of PHH3$^+$ cells in the ventral telencephalon. Data represent means ± SD ($n = 10$, $^*P < 0.05$, one-way ANOVA). Scale bars, (A) 100 µm [applies to (B), (C), (E1) to (G5), and (I) to (N)]; CP, cortical plate; LV, lateral ventricle.

B1 to D5), indicating that the target was region specific. The lowest effective dose (10 mg per mouse) was therefore used in all of the experiments in this study.

Encircling the lateral ventricle is a rich tube-like plexus of vessels (*1*, *2*), which serves as a niche for neuronal proliferation and migration. This unique curved profile of vessels can be observed even in 20-μm-thick sections from saline controls (Fig. 1I) but was disrupted in the ganglionic eminence of the saline-treated *Gabrb3*^{ECKO} telencephalon (Fig. 1J). In NAD$^+$-treated *Gabrb3*^{ECKO} telencephalon, these uniform vascular patterns were restored (Fig. 1K) reinforcing its positive effects on in vivo angiogenesis. Cell proliferation was analyzed in the ventral telencephalon by examining interkinetic nuclear migration with phosphohistone H3 (PHH3), a specific marker for cells undergoing mitosis (Fig. 1, L to O). Abnormal PHH3$^+$ profiles were observed in the saline-treated *Gabrb3*^{ECKO} telencephalon (Fig. 1M) when compared to saline-treated controls (Fig. 1L). NAD$^+$ treatment significantly increased the number of PHH3$^+$ cells at the ventricular zone/subventricular zone surface of *Gabrb3*^{ECKO} ventral telencephalon, indicative of increased endothelial and neuronal cell proliferation (Fig. 1N). Together, these results stimulated our curiosity since the MGE plays a key role in contributing GABAergic interneuron populations to the developing neocortex (*13*–*15*). In addition, several new questions emerged as to the identity and significance of this NAD$^+$-induced cellular architecture in the *Gabrb3*^{ECKO} telencephalon.

Prenatal NAD$^+$ treatment promotes GABAergic neuronal development and migration

We next evaluated the significance of the prenatal NAD$^+$ treatment on cellular mechanisms in the E18 *Gabrb3*^{ECKO} telencephalon with comparisons to the saline-treated groups. We tested for the expression of the homeodomain protein NKX2.1 that is specifically expressed by MGE progenitors (*16*) and is selective to cells of the ventral telencephalon (preoptic area, MGE, globus pallidus, septum, and amygdala). *Nkx2.1* mutants lack an MGE and have interneuron loss in the cerebral cortex (*16*). *Nkx2.1* also acts as a cell fate determinant in regulating the differential migration of cortical and striatal GABAergic interneurons (*17*). We observed a significant reduction of NKX2.1 expression in the MGE of the saline-treated *Gabrb3*^{ECKO} telencephalon (Fig. 2, B and D) when compared to the saline-treated *Gabrb3*$^{fl/fl}$ telencephalon (Fig. 2, A and D). Abnormally, higher expression of NKX2.1 was observed in the globus pallidus, which may be indicative of arrested or stalled migration, and GABAergic neurons are therefore more likely to remain in the basal forebrain (Fig. 2B). This abnormal NKX2.1 profile in the *Gabrb3*^{ECKO} ventral telencephalon was rescued by the prenatal NAD$^+$ treatment. NKX2.1 expression was significantly enriched in the MGE of the NAD$^+$-treated *Gabrb3*^{ECKO} telencephalon (Fig. 2, C and D). We also tested, for expression of PROX1 (prospero homeobox 1), a marker that defines LGE/CGE/POA (lateral ganglionic eminence/caudal ganglionic eminence/preoptic area)–derived cortical interneurons and is expressed in dividing precursors, immature migrating interneurons, as well as mature fully integrated cells (*18*). While the saline-treated *Gabrb3*$^{fl/fl}$ telencephalon showed a normal PROX1 profile (Fig. 2, E and H), a decrease in PROX1 immunoreactivity was observed in saline-treated *Gabrb3*^{ECKO} telencephalon (Fig. 2, F and H). PROX1 expression was significantly increased in the NAD$^+$-treated *Gabrb3*^{ECKO} telencephalon (Fig. 2, G and H). The profile of GABAergic neurons, examined with GABA immunoreactivity, was reduced in saline-treated *Gabrb3*^{ECKO} telencephalon (Fig. 2, J and L) but was restored in NAD$^+$-treated *Gabrb3*^{ECKO} telencephalon (Fig. 2, K and L) similar to the control (Fig. 2, I and L). These results provided novel evidence that, in addition to the improvement in vascular profiles and cell proliferation in the ganglionic eminence, the distinct cellular architecture observed in the MGE of the NAD$^+$-treated *Gabrb3*^{ECKO} telencephalon was pro-GABAergic and consisted of NKX2.1$^+$ and PROX1$^+$ cells with significance for GABAergic neuronal development.

To test whether the prenatal NAD$^+$ treatment was able to influence GABAergic neuronal migration, we performed an in vitro neuronal migration assay (Fig. 2M), after the in vivo NAD$^+$ treatment paradigm (E12 to E17). GABAergic neurons were isolated from the three groups at E18 by using established methodology (*5*) and seeded in culture inserts in the center of 35-mm laminin-coated culture dishes (Fig. 2, M and N1 to N3). β-Tubulin$^+$ neurons from saline controls and NAD$^+$-treated *Gabrb3*^{ECKO} groups migrated robustly (Fig. 2, N1, N3, and O), unlike neurons from the saline-treated *Gabrb3*^{ECKO} group (Fig. 2, N2 and O), both in terms of cell number and distance. These results implicated that the prenatal NAD$^+$ treatment was able to improve the intrinsic capacity of neuronal migration in *Gabrb3*^{ECKO} neurons. We explored this aspect further by using our E12 to E17 NAD$^+$ injection paradigm in glutamate decarboxylase 65–green fluorescent protein (GAD65-GFP) knock-in mice (Fig. 2, P to T). Images of GFP$^+$ cells that had entered the dorsal telencephalon at E18 were collected and analyzed. A visual inspection of the sections revealed an increase in the distribution of the GFP$^+$ cells in the NAD$^+$-treated group (Fig. 2, Q and S) versus the NAD$^+$-untreated group (Fig. 2, P and R). Numerous GFP$^+$ cells were found extending throughout the lateral to medial expanse of the NAD$^+$-treated dorsal telencephalon (Fig. 2, R and S). Quantification also revealed a significant increase in the percentage of GFP$^+$ cells in the NAD$^+$-treated telencephalon (Fig. 2T). These data suggested that prenatal administration of NAD$^+$ can regulate neuronal migration and will be beneficial in disease models in which deficits in GABAergic neuronal development and migration are reported.

We next tested whether the prenatal rescue of blood vessel densities, angiogenesis, and GABAergic neuronal profiles by NAD$^+$ will persist in the adult *Gabrb3*^{ECKO} cerebral cortex (Fig. 2, U and Y). The vascular and GABA cell deficit observed in the saline-treated *Gabrb3*^{ECKO} embryonic brain (Figs. 1, B and D, and 2, J and L) was also recapitulated in the saline-treated *Gabrb3*^{ECKO} prefrontal cortex (P90) as expected (Fig. 2, V, X, and Y). However, a concurrent increase in blood vessel densities and GABAergic interneurons was observed in the NAD$^+$-treated *Gabrb3*^{ECKO} cerebral cortex (Fig. 2, W, X, and Y) and was comparable to saline-treated controls (Fig. 2, U, X, and Y) indicative of long-lasting rescue initiated by the prenatal NAD$^+$ treatment. Collectively, these results implicated a rescue of endothelial and neuronal cellular mechanisms by prenatal NAD$^+$ treatment in the *Gabrb3*^{ECKO} forebrain and raised new questions about the molecular mechanisms of NAD$^+$ action and rescue.

NAD$^+$-mediated rescue of gene expression profiles in *Gabrb3*^{ECKO} telencephalon

To gain deeper insights into NAD$^+$-mediated specific actions in the subcortical telencephalon, we microdissected the MGE and striatal tissue from telencephalic slices of saline-treated *Gabrb3*$^{fl/fl}$ mice, saline-treated *Gabrb3*^{ECKO} mice, and NAD$^+$-treated *Gabrb3*^{ECKO} mice at E18, extracted RNA, and performed microarray hybridization on Mouse Gene 2.0 ST arrays (Affymetrix) and subsequent gene expression analysis (Fig. 3A). Principal components analysis (PCA)

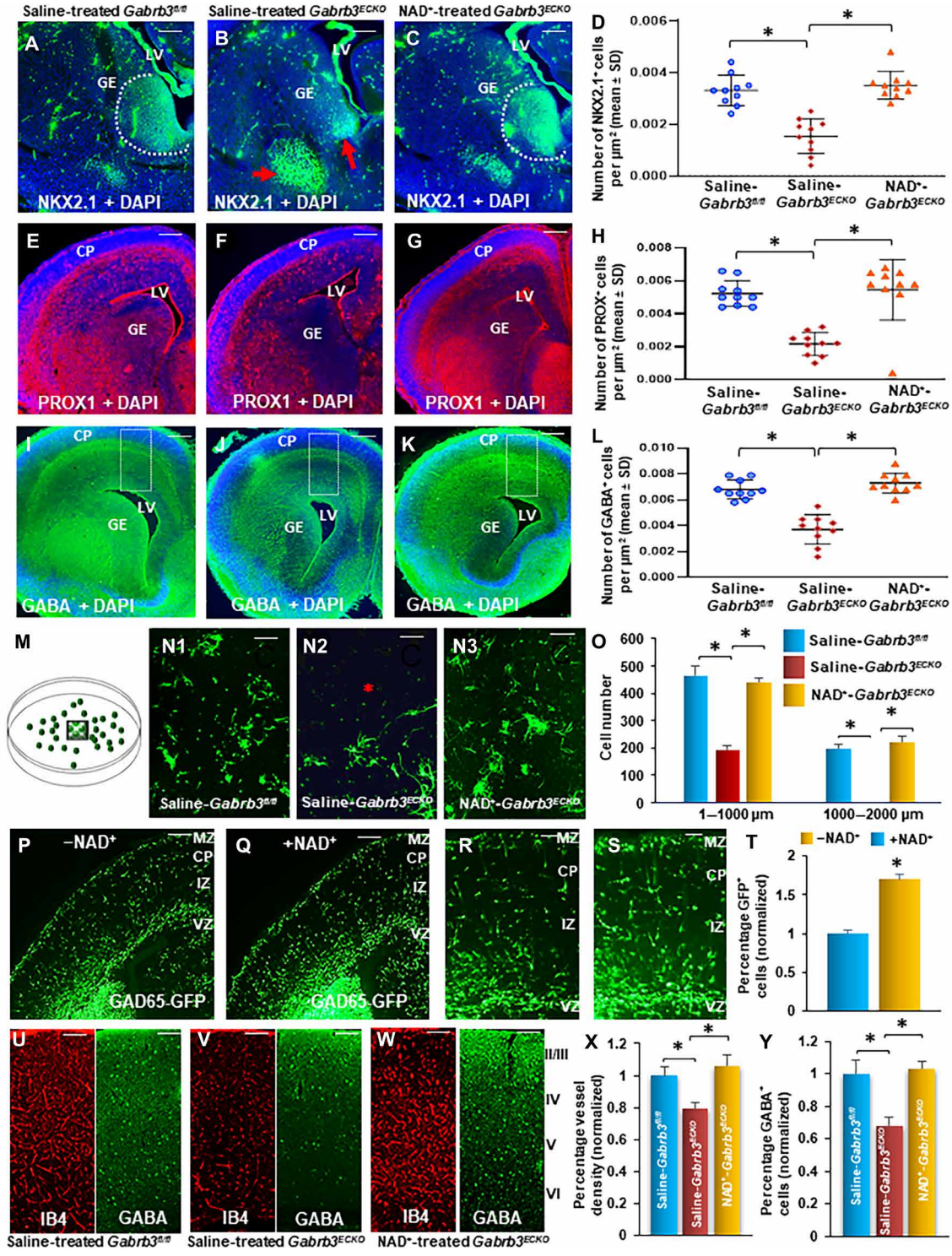

Fig. 2. Cellular mechanisms of NAD$^+$ rescue in the *Gabrb3*^{ECKO} telencephalon. (**A** to **K**) Robust NKX2.1 (A to C), PROX1 (E to G), and GABA (I to K) expression profiles in saline-treated *Gabrb3*$^{fl/fl}$ (A, E, and I) and NAD$^+$-treated *Gabrb3*^{ECKO} (C, G, and K) telencephalon versus abnormal or reduced expression in saline-treated *Gabrb3*^{ECKO} telencephalon [red arrows, (B); (F) and (J)]. (D, H, and **L**) Quantification of NKX2.1$^+$ cells in MGE, PROX1$^+$ cells in ventral telencephalon, and GABA$^+$ neurons in dorsal telencephalon (dotted box), ($n = 10$, $^*P < 0.05$, one-way ANOVA). (**M** to **O**) Schematic of neuronal migration assay. (N1 to N3) Robust neuronal migration in saline-control and NAD$^+$-*Gabrb3*^{ECKO} groups unlike saline-*Gabrb3*^{ECKO} group (red asterisk). (O) Quantification of cell migration ($n = 3$, $^*P < 0.05$, one-way ANOVA). (**P** to **S**) Low-magnification (P and Q) and high-magnification (R and S) images of E18 telencephalic GAD65-GFP$^+$ cells with (Q and S) or without (P and R) NAD$^+$ treatment. MZ, marginal zone. (**T**) Quantification of GAD65-GFP$^+$ cells ($n = 10$, $^*P < 0.05$, Student's *t* test). (**U** to **Y**) Concurrent reduction of vessels and GABAergic neurons in saline-treated *Gabrb3*^{ECKO} prefrontal cortex (V, X, and Y) compared to the other groups (U, W, X, and Y). Quantification depicted in (X) and (Y) ($n = 10$, $^*P < 0.05$; one-way ANOVA). All data represent means ± SD. Scale bars, 100 µm [(A) to (C), (E) to (G), (I) to (K), (N1) to (N3), (P), (Q), and (U) to (W)]; 50 µm [(R) and (S)]. IZ, intermediate zone; VZ, ventricular zone.

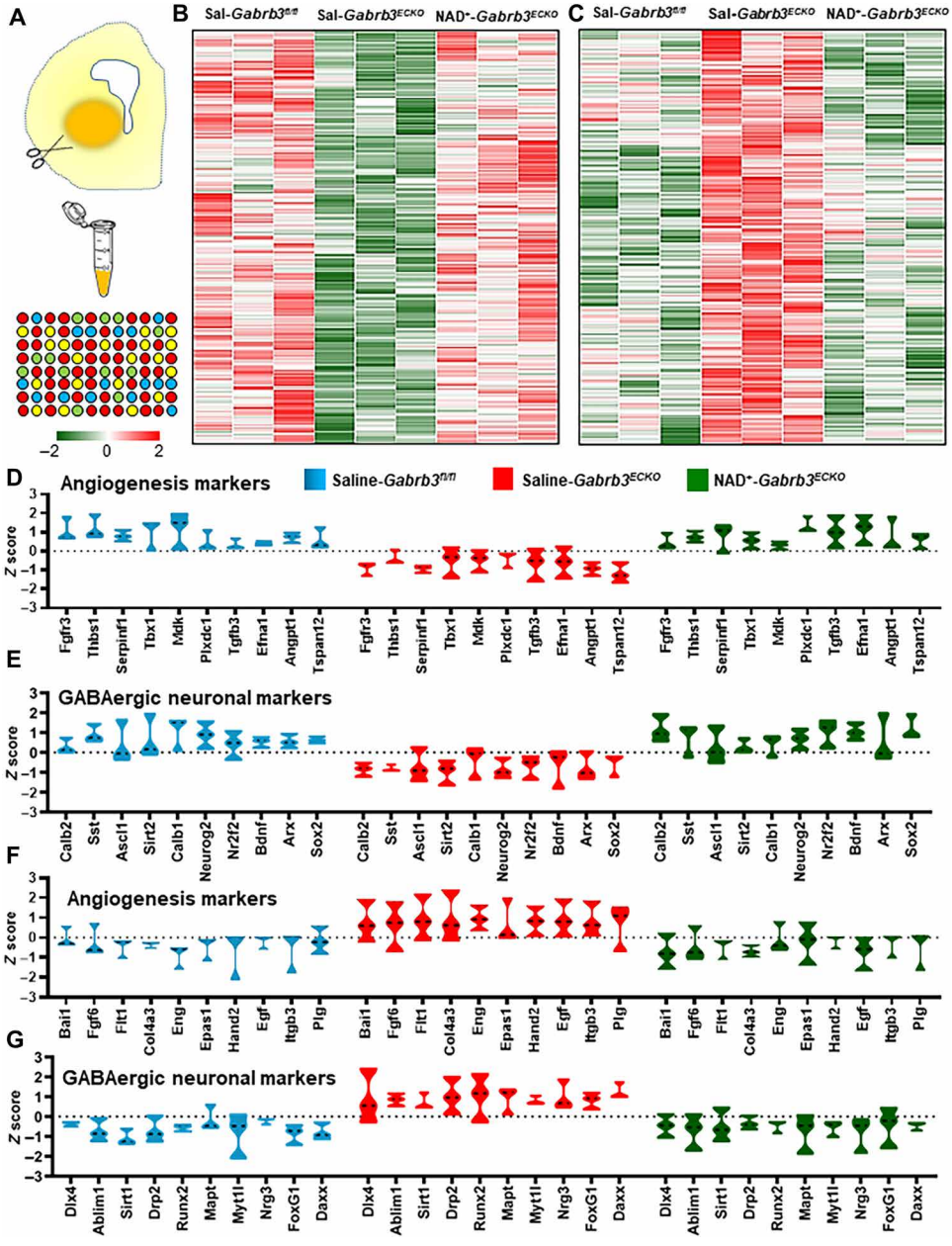

Fig. 3. Rescue of gene expression profiles in NAD$^+$-treated *Gabrb3^{ECKO}* telencephalon. (**A**) Schematic depicting microdissection of MGE and striatal region from the subcortical telencephalon of saline-treated *Gabrb3$^{fl/fl}$*, saline-treated *Gabrb3^{ECKO}*, and NAD$^+$-treated *Gabrb3^{ECKO}* groups ($n = 3$), cell isolation, RNA preparation, and subsequent microarray hybridization. (**B** and **C**) Heatmap clusters depicting down-regulation (B) or up-regulation (C) of genes in saline-treated *Gabrb3^{ECKO}* telencephalon versus saline-treated *Gabrb3$^{fl/fl}$* telencephalon and NAD$^+$-treated *Gabrb3^{ECKO}* telencephalon. (**D** to **G**) Violin plot comparison of top 10 down-regulated (D and E) and up-regulated (F and G) genes in "angiogenesis" and "GABAergic neuronal" categories in saline-treated *Gabrb3^{ECKO}* telencephalon versus saline-treated *Gabrb3$^{fl/fl}$* telencephalon and NAD$^+$-treated *Gabrb3^{ECKO}* telencephalon.

plots depicted strict clustering of triplicates from the three samples in the three-dimensional PCA table (fig. S4A). Differentially expressed genes (fold change cutoff $\geq \pm 50\%$) in the three groups were compared and represented as heatmaps (Fig. 3, B and C). Heatmap clusters depicted a shift in the gene expression profile in the NAD$^+$-treated *Gabrb3^{ECKO}* group versus the saline-treated *Gabrb3^{ECKO}* group, and it was similar to the control group for up-or down-regulated gene sets (Fig. 3, B and C). These results implied that NAD$^+$ had the potential to significantly alter gene expression in the embryonic brain. Gene Ontology (GO) biological process analysis revealed that genes sets in categories such as "DNA repair," "homeostasis," "cell cycle," "transcription," "cell differentiation," "angiogenesis," "cell proliferation," "cell adhesion," "blood vessel development," "blood vessel morphogenesis," "positive regulation of cell migration," "calcium in transport," and several others were comparable between the control and NAD$^+$-treated *Gabrb3^{ECKO}* group (fig. S4B). Several genes related to inflammation were up-regulated in the saline-treated *Gabrb3^{ECKO}* group, which were restored to

normal levels in the NAD$^+$-treated group (fig. S4C). Genes were further classified into specific categories that are essential for embryonic forebrain development: angiogenesis, neurogenesis, GABA signaling, and GABA transcription–related genes, and the top differentially expressed genes in each category are shown (fig. S5). The gene expression profile revealed that the NAD$^+$ treatment had far-reaching consequences for critical events during brain development and can modulate signaling events at the level of extracellular receptors, ion channels, transporters, intracellular signaling molecules, and transcription factors (figs. S4 and S5). In addition, differential expression of 10 marker genes in angiogenesis and GABAergic neuron categories in saline-treated *Gabrb3*$^{fl/fl}$, saline-treated *Gabrb3*^{ECKO}, and NAD$^+$-treated *Gabrb3*^{ECKO} groups was represented as violin plots (Fig. 3, D to G). Genes necessary for blood vessel morphogenesis (*Fgfr3*), homeostatic functions in the regulation of angiogenesis (*Thbs1* and *Serpinf1*), vascular sprouting, integrity and survival (*Tbx1* and *Angpt1*), mitotic factors (*Mdk*), vascular cell proliferation and differentiation (*Plxdc1* and *Efna1*), and blood-brain barrier development (*Tspan12*) were significantly down-regulated in the saline-treated *Gabrb3*^{ECKO} group but were restored to normal levels in the NAD$^+$-treated *Gabrb3*^{ECKO} group (Fig. 3D). Similarly, GABA neuronal subtype–related genes (*Calb2*, *Sst*, and *Calb1*) and GABAergic neuronal development genes (*Sirt2*, *Ascl1*, *Nr2f2*, *Bdnf*, *Arx*, and *Sox2*) that were significantly down-regulated in the saline-treated *Gabrb3*^{ECKO} group were rescued in the NAD$^+$-treated *Gabrb3*^{ECKO} group (Fig. 3E) similar to the saline control group. In addition, other genes required for vascular development and angiogenesis (*Fgf6*, *Flt1*, *Hand2*, *Egf*, *Itgb3*, and *Plg*), hypoxia-related (*Epas1*), as well as negative regulators of angiogenesis (*Bai1*, *Col4a3*, and *Eng*) that were up-regulated in the saline-treated *Gabrb3*^{ECKO} group were restored to normal expression levels in the NAD$^+$-treated *Gabrb3*^{ECKO} group (Fig. 3F). Likewise, several GABAergic pathway regulatory genes (*Dlx4*, *Sirt1*, *Drp2*, *Foxg1*, and *Daxx*) and axon guidance–related genes (*Ablim1*, *Nrg3*) that were up-regulated in the saline-treated *Gabrb3*^{ECKO} group were restored to normal expression levels in the NAD$^+$-treated *Gabrb3*^{ECKO} group (Fig. 3G). Collectively, these results indicate that extensive molecular changes occurred in endothelial and neuronal cell types in the *Gabrb3*^{ECKO} telencephalon that were rescued by the prenatal NAD$^+$ treatment.

Mechanistic insights into NAD$^+$ action on *Gabrb3*^{ECKO} endothelial cells

To gain mechanistic insights into NAD$^+$ action on endothelial cells, we specifically isolated periventricular endothelial cells from saline-treated *Gabrb3*$^{fl/fl}$, saline-treated *Gabrb3*^{ECKO}, and NAD$^+$-treated *Gabrb3*^{ECKO} groups at the end of the treatment paradigm and tested for notable changes in gene expression that were observed in the microarray data by performing quantitative real-time polymerase chain reaction (qRT-PCR). We found that the prenatal NAD$^+$ treatment had restored the expression of several critical regulators of angiogenesis in *Gabrb3*^{ECKO} endothelial cells, for instance, *Tek*, *vWF*, *F2r*, *Sirt2*, *Nos1*, and *Pax6* (fig. S6, A to G). GABA is synthesized from glutamate by *Gad* genes. The glutamic acid decarboxylase isoforms *Gad1* and *Gad2* were concurrently rescued in *Gabrb3*^{ECKO} endothelial cells (fig. S6, H and I). The qRT-PCR gene expression levels followed a similar trend with that of the levels in the microarray data, reinforcing that the whole-tissue microarray was capable of highlighting some endothelial cell–specific gene changes (fig. S6). These data indicate that NAD$^+$ is able to directly modulate intracellular GABA levels in *Gabrb3*^{ECKO} endothelial cells. Together, our results implicate NAD$^+$ as a critical modulator of angiogenesis in the embryonic forebrain.

Endothelial cell–derived GABA plays dual roles in the embryonic forebrain. It not only activates a positive feedback cycle in endothelial cells that stimulates angiogenesis but also is an essential chemoattractive and guidance cue for promotion of long-distance migration of GABAergic interneurons (*1*). Endothelial cell–specific deletion of *Gabrb3* significantly decreased GABA expression and secretion in embryonic periventricular endothelial cells (*1*). Since *Gad1* and *Gad2* were rescued in *Gabrb3*^{ECKO} endothelial cells by the prenatal NAD$^+$ treatment (fig. S6, H and I), we tested whether GABA expression was rescued in *Gabrb3*^{ECKO} endothelial cells (Fig. 4, A to C). Control endothelial cells typically form tight networks or clusters under normal culture conditions. We observed robust GABA expression by immunohistochemistry (IHC) in periventricular endothelial cells from the saline control group, and these cells also showed robust cluster formation (Fig. 4A). Saline-treated *Gabrb3*^{ECKO} endothelial cells, in sharp contrast, showed a marked reduction in GABA expression, and these cells did not form good clusters (Fig. 4B). Prenatal NAD$^+$ treatment significantly improved cluster formation in *Gabrb3*^{ECKO} endothelial cells, and GABA expression was also restored (Fig. 4C). Next, we investigated the secretion of GABA by enzyme-linked immunosorbent assay (ELISA) in the three groups. As expected, there was a significant reduction in GABA secretion from saline-treated *Gabrb3*^{ECKO} endothelial cells (Fig. 4D), and this was rescued in NAD$^+$-treated *Gabrb3*^{ECKO} endothelial cells and was similar to the saline control (Fig. 4D). *Daxx*, a transcriptional repressor of *Gad* genes (*19*–*21*) that synthesizes GABA (Fig. 4, E to H), was modulated by the NAD$^+$ treatment. *Daxx* mRNA and protein levels were up-regulated in *Gabrb3*^{ECKO} endothelial cells (Fig. 4, E, G, and I), as a result of which GABA expression and consequently secretion is affected. NAD$^+$ is directly able to regulate *Daxx* and normalize DAXX levels (Fig. 4, E, H, and I), because of which GABA expression (Fig. 4C) and secretion (Fig. 4D) seem to be restored. These results confirmed that the prenatal NAD$^+$ treatment can directly modulate synthesis and release of GABA in endothelial cells. Thus, endothelial cell–secreted GABA that is essential to promote neuronal migration was rescued in the NAD$^+$-treated *Gabrb3*^{ECKO} group.

An important aspect that influences endothelial cell proliferation is Ca^{2+} influx, which is important for cell cycle progression in the neocortex (*22*). $GABA_A$ receptor activation in *Gabrb3*$^{fl/fl}$ periventricular endothelial cells leads to an influx of Ca^{2+} that influences cell proliferation (*1*). However, in *Gabrb3*^{ECKO} periventricular endothelial cells, because of the deletion of the β3 subunit, the $GABA_A$ receptors are dysfunctional (*1*). Therefore, the autocrine feedback loop of GABA acting on $GABA_A$ receptors will not work in these *Gabrb3*^{ECKO} endothelial cells to cause Ca^{2+} influx, even if GABA secretion is restored. In the absence of this mechanism, we questioned whether the prenatal NAD$^+$ treatment was able to activate alternate mechanisms to trigger Ca^{2+} influx in *Gabrb3*^{ECKO} endothelial cells. The gene expression profiling analysis (Fig. 3) gave us new leads. We found that calcium signaling–related gene expression in the NAD$^+$-treated *Gabrb3*^{ECKO} subcortical telencephalon was similar to the control group for up- or down-regulated gene sets when compared to the saline-treated *Gabrb3*^{ECKO} group (fig. S7, A and B). We validated the rescue of several calcium signaling genes (*Grin2a*, *Trpm2*, *Trpc4*, and *Trpv6*) specifically in NAD$^+$-treated *Gabrb3*^{ECKO}

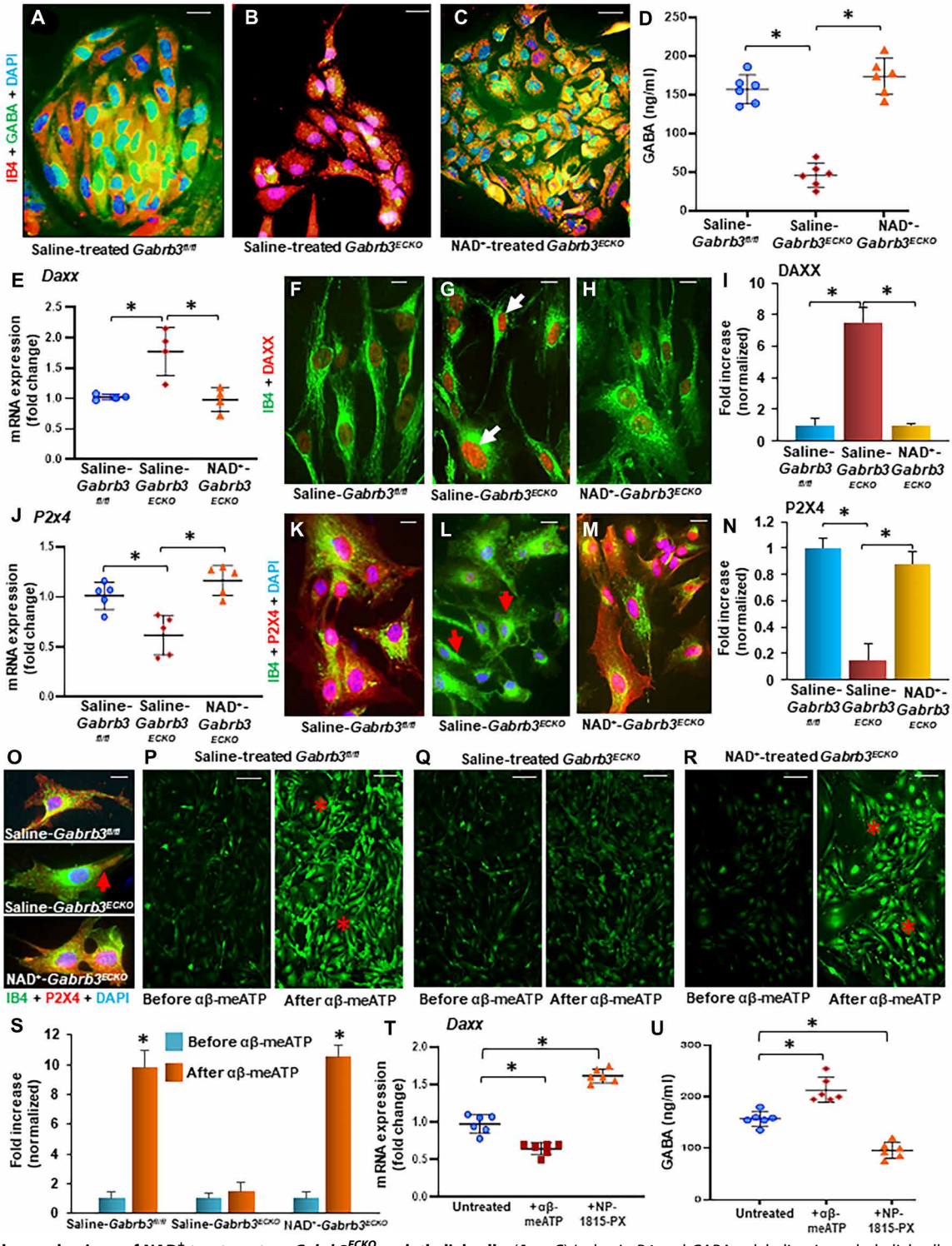

Fig. 4. Molecular mechanisms of NAD$^+$ treatment on *Gabrb3^{ECKO}* endothelial cells. (**A** to **C**) Isolectin B4 and GABA colabeling in endothelial cells from the three groups. (**D**) Quantification of GABA secretion measured by ELISA; data represent means ± SD ($n = 6$, *$P < 0.05$, one-way ANOVA). (**E** to **N**) RT-qPCR validation of *Daxx* and *P2x4* mRNA expression [(E) and (J); $n = 3$, *$P < 0.05$, one-way ANOVA], DAXX (F to H) and P2X4 (K to M) protein expression and quantification [(I) and (N); $n = 10$, *$P < 0.05$, one-way ANOVA] in endothelial cells from the three groups. Data represent means ± SD. (**O**) High-magnification images of P2X4 expression in endothelial cells from the three groups. (**P** to **R**) Calcium imaging shows no increase in intracellular calcium following αβ-meATP application, in saline-treated *Gabrb3^{ECKO}* endothelial cells (Q) when compared to the other two groups [red asterisks, (P) and (R)]. (**S**) Quantification of calcium imaging data; data represent means ± SD ($n = 10$, *$P < 0.05$, one-way ANOVA). (**T** and **U**) Quantification of Daxx mRNA expression (T) and GABA secretion measured by ELISA (U) after culturing wild-type endothelial cells in the presence of a P2X4 receptor agonist (αβ-meATP) or antagonist (+NP-1815-PX). Data represent means ± SD, ($n = 6$, *$P < 0.05$, one-way ANOVA). Scale bars, 100 μm [(A) to (C) and (P) to (R)]; 50 μm [(F) to (H) and (K) to (M)].

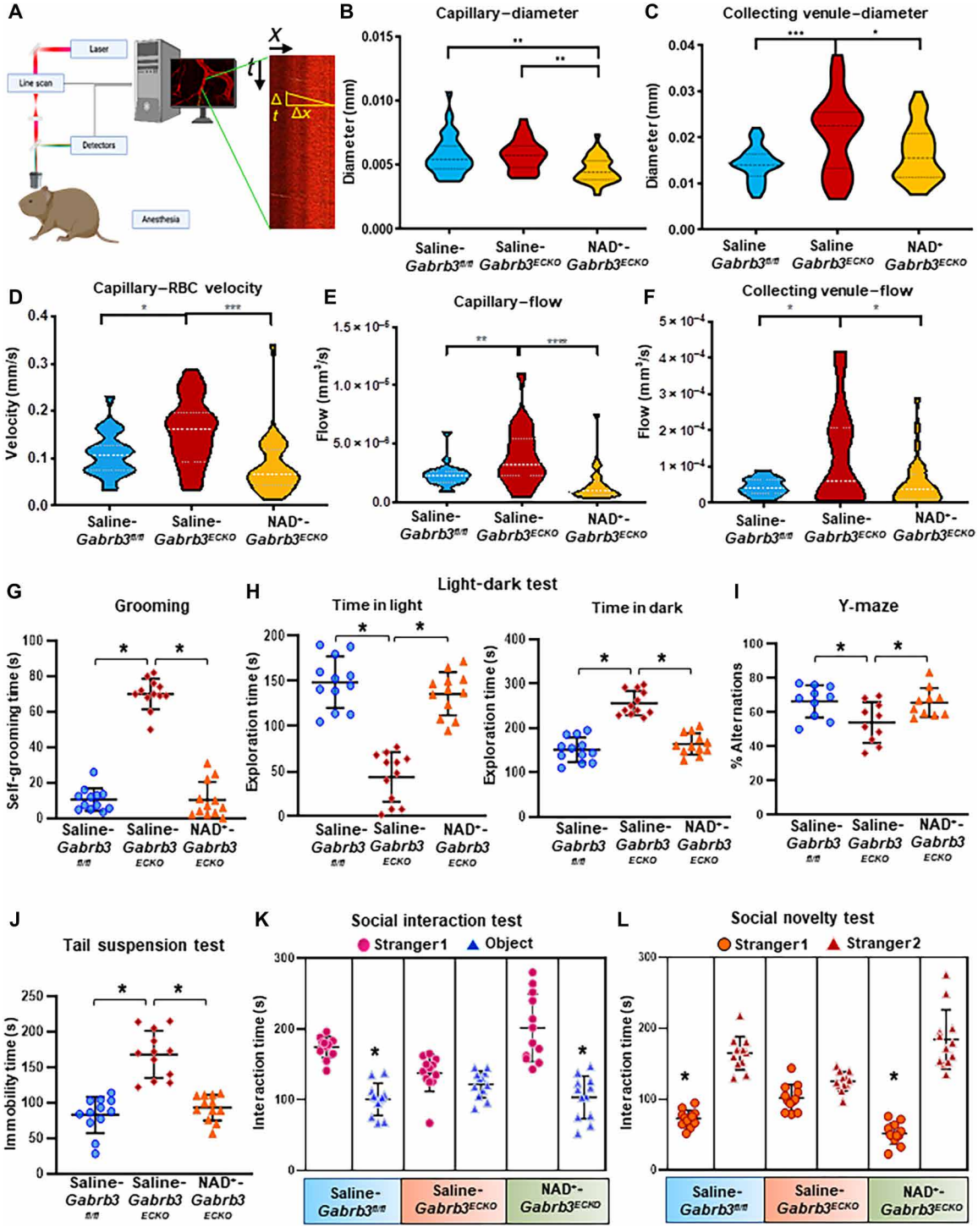

Fig. 5. Rescue of blood flow and abnormal behaviors in *Gabrb3*^{ECKO} adult brain after the prenatal NAD$^+$ treatment. (**A**) Schematic of blood flow velocity acquisition by MPLSM. Dark streaks (negative contrast) correspond RBCs moving along the central axis of the blood vessel. The slopes of these streaks correspond to the RBC velocities. (**B** to **F**) Violin plots showing distribution of capillary diameter [(B), $n = 40$, $n = 31$, $n = 39$ vessels], collecting venule diameter [(C), $n = 35$, $n = 26$, $n = 38$ vessels], RBC velocities (D) and blood flow (E) in capillaries ($n = 40$, $n = 31$, $n = 39$ vessels) and blood flow in collecting venules [(F), $n = 35$, $n = 26$, $n = 38$ vessels], across the three mouse groups, respectively. Data are presented in violin plots showing median, quartiles, and distribution (*$P < 0.05$, **$P < 0.005$, ***$P < 0.0005$ one-way ANOVA). (**G** to **L**) Quantification of self-grooming time (G), exploration time in light-dark test (H), spontaneous alteration in Y-maze (I), immobility time in tail suspension test (J), and interaction time in social interaction (K) and social novelty (L) tests all showed significant improvement in behavior in NAD$^+$-treated *Gabrb3*^{ECKO} mice when compared to saline-treated *Gabrb3*^{ECKO} mice and was comparable to saline-treated *Gabrb3*$^{fl/fl}$ mice. For all behavioral tests (G to L), data represent means ± SD ($n = 12$, *$P < 0.05$, ****$P < 0.0001$, one-way ANOVA).

periventricular endothelial cells, and it was comparable to the microarray results (fig. S7, C to F). We also observed a notable change in purinergic receptor signaling genes in the NAD^+-treated $Gabrb3^{ECKO}$ group when compared to the saline-treated $Gabrb3^{ECKO}$ group (fig. S7, A and B). Therefore, we validated P2X4 expression at both mRNA and protein levels in periventricular endothelial cells, prepared after the 6-day saline and NAD^+ treatment paradigm (Fig. 4, J to O). P2X4 has been reported as the most abundantly expressed P2X receptor subtype in vascular endothelial cells from several tissues, and its deficiency affects normal endothelial cell responses, such as Ca^{2+} influx (*23*). However, P2X4 expression and functional significance in embryonic forebrain endothelial cells are unknown. We found that P2X4 mRNA and protein were robustly expressed in saline-treated $Gabrb3^{fl/fl}$ endothelial cells (Fig. 4, J, K, and N). P2X4 mRNA and protein expression were significantly decreased in saline-treated $Gabrb3^{ECKO}$ endothelial cells (Fig. 4, J, L, and N), but its expression was rescued in NAD^+-treated $Gabrb3^{ECKO}$ endothelial cells (Fig. 4, J, M, and N). To test whether P2X4 receptor activation on endothelial cells leads to an influx of Ca^{2+}, we incubated periventricular endothelial cells from the three groups in the presence of αβ-meATP (alpha,beta-methylene ATP) that has been reported to show agonist activity at P2X receptors, including P2X4 (Fig. 4, N to Q) (*24*, *25*). Application of αβ-meATP produced a significant increase in intracellular calcium in saline-treated $Gabrb3^{fl/fl}$ endothelial cells and NAD^+-treated $Gabrb3^{ECKO}$ endothelial cells in calcium imaging assays that were further quantified (Fig. 4, P, R, and S). However, there was no marked increase in intracellular calcium in saline-treated $Gabrb3^{ECKO}$ endothelial cell proliferation after αβ-meATP application (Fig. 4, Q and S). Application of potent agonists for the P2X7 receptor Bz-ATP (benzoylbenzoyl-ATP) and for the P2Y13 receptor 2Me-SADP (2-Methylthioadenosine diphosphate trisodium salt) (*25*) also produced an influx of Ca^{2+} (fig. S8, A to H); therefore, multiple purinergic receptor subtypes seem to be activated by NAD^+. A rescue of P2X7 and P2Y13 mRNA expression was also observed after the NAD^+ treatment (fig. S8, I and J). We next activated or inactivated P2X4 receptors in cultured wild-type periventricular endothelial cells, by incubating the endothelial cells in the presence of agonist αβ-meATP or antagonist +NP-1815-PX, followed by testing for *Daxx* mRNA expression and GABA secretion by ELISA. Activation of purinergic receptors reduced *Daxx* expression and increased GABA secretion, while inhibition of purinergic receptors increased *Daxx* expression and reduced GABA secretion (Fig. 4, T and U). These results indicate an inverse correlation between *Daxx* expression and GABA secretion that is modulated directly by purinergic receptor signaling. Together, these results indicate that purinergic receptor signaling is restored in $Gabrb3^{ECKO}$ periventricular endothelial cells after NAD^+ treatment and elucidates an alternate mechanism for NAD^+-mediated rescue of endothelial cell proliferation and angiogenesis in the prenatal developmental period.

Prenatal NAD^+ treatment rescued adult brain blood flow and ameliorated abnormal behaviors in the $Gabrb3^{ECKO}$ mice

The consequences of loss of endothelial *Gabrb3* in the embryonic brain persisted in the adult brain, reflecting as reduced vascular densities and functional changes in blood vessels as well as a reduction of cortical interneurons (*1*). This resulted in multifaceted behavioral deficits that are common to several different psychiatric diseases, with symptoms that included impaired reciprocal social interactions, communication deficits, and heightened anxiety (*1*). Since the prenatal NAD^+ treatment mediated rescue of cellular and molecular aspects of the $Gabrb3^{ECKO}$ embryonic brain (Figs. 1 to 4) and restored the vascular and GABAergic neuronal deficits in the adult cerebral cortex (Fig. 2, U to Y), we questioned whether it could contribute to a rescue of blood flow and amelioration of abnormal behaviors.

Therefore, we evaluated vessel diameters, red blood cell (RBC) velocity and blood flow in the cerebral cortex of saline-treated $Gabrb3^{fl/fl}$ mice, saline-treated $Gabrb3^{ECKO}$ mice, and NAD^+-treated $Gabrb3^{ECKO}$ mice (Fig. 5, A to F) using multiphoton laser-scanning microscopy (MPLSM) (*26*–*28*) and a sophisticated cranial window model. An increase in the diameter of capillaries and collecting venules was observed in the saline-treated $Gabrb3^{ECKO}$ mice compared to saline-treated $Gabrb3^{fl/fl}$ mice (Fig. 5, B and C). This morphological alteration was rescued in NAD^+-treated $Gabrb3^{ECKO}$ mice (Fig. 5, B and C). Similarly, RBC velocity was significantly increased in capillaries in saline-treated $Gabrb3^{ECKO}$ mice when compared to saline-treated $Gabrb3^{fl/fl}$ mice, and this was reversed in NAD^+-treated $Gabrb3^{ECKO}$ mice (Fig. 5D). Consistently, blood flow in capillaries and collecting venules was also significantly reduced in NAD^+-treated $Gabrb3^{ECKO}$ mice when compared to saline-treated $Gabrb3^{ECKO}$ mice (Fig. 5, E and F). Histograms depict the changes in blood flow distribution in capillaries and collecting venules between the three groups (fig. S9, A to F). No significant changes were observed in vessel diameter, RBC velocity, or blood flow in the postcapillary venules of saline-treated $Gabrb3^{ECKO}$ mice when compared to controls (fig. S9, G to L). These results indicate that the capillaries and the collecting venules were the most significantly affected units of the microcirculation in saline-treated $Gabrb3^{ECKO}$ mice that were rescued by the prenatal NAD^+ treatment.

The prenatal NAD^+ treatment did not have any effect on litter size, and pups grew normally to adulthood. We therefore performed behavioral tests to screen for stress, anxiety, locomotion, cognition, and sociability in saline-treated $Gabrb3^{fl/fl}$ mice, saline-treated $Gabrb3^{ECKO}$ mice, and NAD^+-treated $Gabrb3^{ECKO}$ mice. Mice from saline- and NAD^+-treated groups were housed individually in cages containing wood chip bedding and two nestlets (pressed cotton) (fig. S10, A to D) or more naturalistic material like shredded paper strips (fig. S10, E to H). Saline-treated $Gabrb3^{ECKO}$ mice showed poor nest-building behavior in both normal (fig. S10, B and D) and enriched (fig. S10, F and H) environments when compared to saline-treated $Gabrb3^{fl/fl}$ mice (fig. S10, A, D, E, and H), indicative of heightened stress/anxiety and impaired home cage social behavior. NAD^+-treated $Gabrb3^{ECKO}$ mice showed significant improvement in their nest-building ability and were comparable to saline control mice (fig. S10, C, D, G, and H). This rescue of home cage social behavior was a robust indication of well-being in NAD^+-treated $Gabrb3^{ECKO}$ mice. The severe grooming behavior indicative of impaired home cage social behavior and increased stress/anxiety in saline-treated $Gabrb3^{ECKO}$ mice was also ameliorated after the prenatal NAD^+ treatment (Fig. 5G).

Anxiety was next assessed with the classic light-dark transition test, which triggers a struggle between the desires to explore a novel environment versus natural aversion of a brightly illuminated open space. While the saline-treated $Gabrb3^{ECKO}$ mice showed an aversion to brightly lit open space and preferred the dark area (Fig. 5H), both saline-treated $Gabrb3^{fl/fl}$ mice and NAD^+-treated $Gabrb3^{ECKO}$ mice made several entries into the brightened space and spent equivalent times between the light and dark sides of the open field (Fig. 5H). Open-field locomotor activity defined as breaking of total or

consecutive infrared photobeams was monitored for 60 min, and no significant differences were observed between the three groups (fig. S10, I and J). The Y-maze spontaneous alternation test was used to evaluate for spatial learning and memory in the three groups of mice. After introduction to the center of the maze, the mice were given free access to all three arms. If a different arm is chosen by the mouse than the one from where it arrived, then this choice is called an alteration and is considered the correct response. The total number of arm entries and the sequence of entries are recorded to calculate the percentage of alternation. Saline-treated *Gabrb3*$^{fl/fl}$ mice and NAD$^+$-treated *Gabrb3*^{ECKO} mice showed a significant increase in percentage alternations when compared to saline-treated *Gabrb3*^{ECKO} mice, indicative of an improvement in cognition (Fig. 5I). Next, we used the tail suspension test to evaluate the mice for depressive behavior. When suspended by their tails, normal mice will struggle to face upward and show apparent escape efforts that include running movements, body torsion, reaching, and shaking. Immobility of the mouse is defined as a depressive state when the mouse has given up and does not want to put in the effort to try to escape. Saline-treated *Gabrb3*^{ECKO} mice showed longer periods of immobility compared to saline control mice (Fig. 5J). NAD$^+$-treated *Gabrb3*^{ECKO} mice had significantly lower immobility times, similar to saline controls (Fig. 5J).

NAD$^+$-treated *Gabrb3*^{ECKO} mice also showed a significant improvement in social communication skills. In a three-chamber social communication test, saline-treated *Gabrb3*^{ECKO} mice showed no preference for a stranger mouse and spent an approximately similar time in investigating the stranger mouse versus an inanimate object, signifying impaired sociability. In contrast, NAD$^+$-treated *Gabrb3*^{ECKO} mice interacted with the stranger mouse for a significantly longer duration than with the inanimate object, similar to saline controls (Fig. 5K). In the social novelty phase, when a new stranger mouse was introduced into the previously empty cylinder, both saline-treated *Gabrb3*$^{fl/fl}$ mice and NAD$^+$-treated *Gabrb3*^{ECKO} mice showed a marked preference for stranger 2 versus the now-familiar stranger 1, while *Gabrb3*^{ECKO} mice did not show such a preference. This is indicative of rescue of social motivation, memory, and novelty exploration in NAD$^+$-treated *Gabrb3*^{ECKO} mice (Fig. 5L). Collectively, these results provide novel evidence that NAD$^+$ treatment during a select prenatal developmental window is sufficient to rescue blood flow in an irreversible manner and ameliorate abnormal behaviors.

DISCUSSION

The results of our studies are notable for several reasons and offer many exciting new perspectives. First, they illustrate the importance of having a greater understanding of cell type–specific origins of neuropsychiatric disorders. Intrinsic defects within forebrain blood vessels from the earliest developmental time points can be a major cause for the origin of psychiatric diseases (*1*–*5*). Telencephalic angiogenesis precludes neuronal development and provides valuable guidance cues for neurogenesis and neuronal migration. Since the endothelial GABA signaling pathway molds telencephalic angiogenesis with significant consequences for neuronal development and, most importantly, is sufficient to cause behavioral dysfunction, a pro-angiogenic strategy to target the problem was our first goal. Rescue of prenatal forebrain angiogenesis was able to trigger a rescue of downstream neurovascular interactions, with significant benefits for brain repair during the critical developmental phase in the *Gabrb3*^{ECKO} mouse model, thereby eliminating behavioral dysfunction.

Administration of NAD$^+$ precursors, nicotinamide riboside, or nicotinamide mononucleotide, serves to increase intracellular levels of NAD$^+$ to restore dysfunctional cellular energy metabolism in mitochondria associated with aging and neurodegenerative conditions (*9*, *10*). Thus, NAD$^+$ decline is well known to act as a trigger for age-associated pathophysiologies, and modulation of intracellular NAD$^+$ levels by NAD precursors represents a strategy to slow down aging and neurodegeneration. In contrast, our studies show that NAD$^+$ administered systemically, or the extracellular NAD$^+$ contribution, exerts different cellular effects from those of the NAD precursors. For instance, NAD$^+$ induced immune homeostasis and reversed multiple sclerosis disease progression by restoring tissue integrity, via stem cell proliferation, remyelination, and neuroregeneration (*6*). Thus, NAD$^+$ can directly cause significant changes in gene expression and can be used for cell repair. Therefore, our second finding was that the use of NAD$^+$ served the purpose of intervention in a psychiatric disease model as early as possible. NAD$^+$, being a small natural molecule, had a very powerful effect on prenatal brain development, when in the right place at the right time. At the cellular level, it stimulated cell proliferation and migration in the *Gabrb3*^{ECKO} telencephalon, key elements that were deficient in this model (Fig. 6, A and B). Furthermore, NAD$^+$ was able to directly modulate gene expression in both *Gabrb3*^{ECKO} endothelial cells and neuronal cells, by restoring it to normal levels. For instance, endothelial cell–derived GABA is a valuable guidance cue, indispensable for long-distance neuronal migration. One way by which NAD$^+$ was able to rescue GABA expression and secretion and thereby rescue the chemoattraction and vascular guidance cue essential for GABAergic neuronal tangential migration was by down-regulation of *Daxx* in *Gabrb3*^{ECKO} endothelial cells (Fig. 6B). It restored the synchrony of the neurovascular communication that is essential for cell migration and final distribution in the prenatal brain, essential events for cortical circuit formation. In addition, by rescuing purinergic receptor signaling in *Gabrb3*^{ECKO} endothelial cells, NAD$^+$ activated an alternate pathway for calcium influx into endothelial cells and to trigger angiogenesis (Fig. 6B). Our data also suggest that modulation of purinergic receptor signaling can regulate Daxx expression and GABA secretion; thereby, NAD$^+$-mediated rescue of purinergic receptor signaling was able to bypass the $GABA_A$ receptor signaling pathway in endothelial cells. NAD$^+$ also had a specific effect on GABAergic neurons in the ganglionic eminence and restored expression of key transcription factors like NKX2.1 and PROX1. Thus, this 6-day prenatal developmental paradigm of exogenous treatment with NAD$^+$ served as a major contributor for the rescue of angiogenesis, GABAergic neuronal migration, and overall brain morphology in the *Gabrb3*^{ECKO} forebrain, with far-reaching consequences after birth for improvement of blood flow and behavioral function (Fig. 6C).

Third, our study highlights that the prenatal NAD$^+$ treatment was sufficient to induce lasting and irreversible morphological changes to blood vessels in the *Gabrb3*^{ECKO} mouse model. The increased blood vessel diameters in the *Gabrb3*^{ECKO} adult cerebral cortex caused an abnormal increase in blood flow. This was reversed intrinsically by the prenatal NAD$^+$ treatment paradigm. This is of high significance, indicative that the NAD$^+$-induced vasoconstriction in the prenatal developmental phase was of a permanent nature. It draws attention to interesting aspects about NAD$^+$ modeling of abnormal nascent or developing blood vessels by purinergic signaling that can be tapped into for permanent repair.

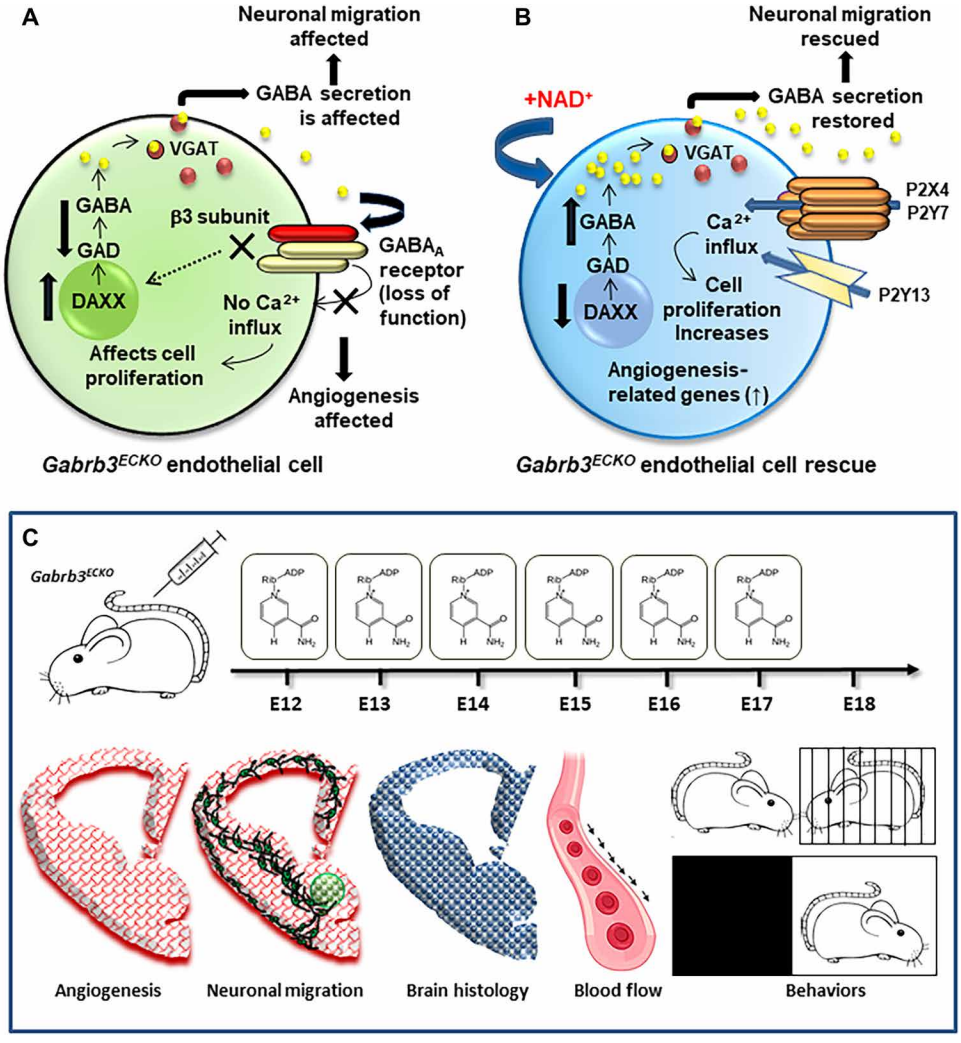

Fig. 6. The significance of NAD$^+$-mediated rescue of telencephalic angiogenesis and brain development. (**A**) Summary schema depicting defects in the positive feedback GABA signaling pathway in *Gabrb3*^{ECKO} endothelial cells, in which due to loss of the β3 subunit, GABA$_A$ receptors become dysfunctional. As a result, endothelial GABA is unable to activate GABA$_A$ receptors and cannot trigger Ca^{2+} influx and endothelial cell proliferation. *Gabrb3* also regulates GABA expression via the transcriptional repressor *Daxx*. *Daxx* expression is up-regulated in *Gabrb3*^{ECKO} endothelial cells; therefore, GABA expression is significantly reduced. This affects GABA secretion from *Gabrb3*^{ECKO} endothelial cells and disturbs paracrine GABA signaling for neuronal migration and autocrine GABA signaling for angiogenesis. VGAT, vesicular GABA transporter. (**B**) The NAD$^+$-mediated rescue of *Gabrb3*^{ECKO} endothelial cells bypasses the GABA$_A$ receptor–GABA signaling autocrine pathway. It acts via purinergic receptor signaling that triggers Ca^{2+} influx and restores cell proliferation in *Gabrb3*^{ECKO} endothelial cells. It causes direct changes to gene expression in *Gabrb3*^{ECKO} endothelial cells. By down-regulating *Daxx*, it restores GABA expression and secretion in *Gabrb3*^{ECKO} endothelial cells and thereby restores neuronal migration. (**C**) Our studies show that the NAD$^+$ prenatal administration paradigm is of great significance for rescuing abnormal embryonic brain development. Rescue of prenatal angiogenesis and brain development in the *Gabrb3*^{ECKO} model improves blood flow and prevents the origin of psychiatric symptoms.

Fourth, our results suggest that there is a NAD$^+$-susceptible site in the MGE of the embryonic telencephalon. Since the MGE contributes some of the most important GABAergic neuronal populations to the cerebral cortex in the prenatal period (*14*, *15*), NAD$^+$ treatment may provide significant benefits in disease scenarios in which GABAergic cell deficits are reported or anticipated. It will be interesting in the future to extend this prenatal NAD$^+$ treatment strategy to new psychiatric disease models that are linked to abnormal brain development. For instance, early inflammation is a well-recognized factor for autism, and NAD$^+$ therapy may show significant benefits in autism models. It also opens new avenues for questioning whether increased NAD$^+$ consumption during the gestational periods in normal mothers may increase GABAergic cell output in the developing forebrain, thereby tipping the balance of excitation-inhibition in the brain and predisposing children to neuropsychiatric diseases.

In the 1960s, nicotinic acid deficiency was considered to produce psychopathological symptoms, and NAD was used as a treatment option for patients with acute and chronic schizophrenia, in concert with nicotinamide or nicotinic acid (*29*–*31*). However, the high-dose ranges administered and variations in NAD preparation gradually became a problem. More recently, a significant reduction in the NAD$^+$/NADH (reduced form of NAD$^+$) ratio was reported in chronically ill patients with schizophrenia, providing evidence for redox imbalance in the brain, reflecting oxidative stress (*32*). Our study offers new perspectives for NAD$^+$ in vascular repair and in modulating endothelial cell–derived GABA levels in the embryonic

forebrain. Prenatal NAD^+ treatment can serve as a proangiogenic, neurovascular strategy to sculpt brain development, prevent the origin of psychiatric symptoms, and offer significant long-term benefits to offspring.

MATERIALS AND METHODS

Animals

Timed pregnant CD1 mice were purchased from Charles River Laboratories, MA. Colonies of GAD65-GFP mice were maintained in our institutional animal facility. *Tie2-cre* mice and *Gabrb3 floxed* (*Gabrb3*$^{fl/fl}$) mice were obtained from the Jackson Laboratory. The *Tie2-cre* transgene is known for uniform expression of cre recombinase in endothelial cells during embryogenesis and adulthood (*1*, *3*). To selectively delete *Gabrb3* in endothelial cells, *Tie2-cre* transgenic mice (males) were crossed to *Gabrb3*$^{fl/fl}$ mice (females) to generate *Tie2-cre; Gabrb3*$^{fl/+}$ mice (males). These were further crossed with *Gabrb3*$^{fl/fl}$ mice (females) to obtain the *Gabrb3* conditional knockouts (*Tie2-cre; Gabrb3*$^{fl/fl}$ mice). The day of plug discovery was designated E0. Animal experiments were in full compliance with the National Institutes of Health Guide for Care and Use of Laboratory Animals and were approved by the Huntington Medical Research Institutes and McLean Institutional Animal Care Committees.

Histology, IHC, and microscopic analysis

Paraffin IHC was performed on embryonic brains only, while frozen section IHC was used on both embryonic and adult brains. Briefly, for paraffin IHC, E18 brains were fixed in zinc fixative (BD Biosciences PharMingen) for 24 hours and processed for paraffin histology. Histological stainings with hematoxylin (Vector Laboratories) and eosin (Sigma-Aldrich) were performed on 8-μm coronal sections. Lectin histochemistry (with biotinylated isolectin B4, 1:50, Sigma-Aldrich) and IHC were performed on 20-μm sections. Primary antibodies used for IHC were as follows: anti-PHH3 (1:200, Millipore) and anti-NKX2.1 (1:50, Sigma-Aldrich) followed by secondary detection with Alexa Fluor conjugates (Invitrogen). 4′,6-Diamidino-2-phenylindole (DAPI) (Vector Laboratories) was used to label nuclei. For frozen-section IHC, E18 and P90 brains were removed, fixed in 4% paraformaldehyde for 24 hours, cryoprotected in sucrose gradient, embedded into optimal cutting temperature medium for frozen blocks, sectioned at 40 μm on a cryostat, and immunostained with anti-GABA (1:80, Sigma-Aldrich) and anti-PROX1 (1:80, Millipore) antibodies. Twenty sections from each brain were used for IHC and histology experiments. Uniform penetration of antibodies or stains throughout the section was ascertained, and the quality of the staining in each digital section was examined. Only those sections that showed uniform labeling were included in further analysis. All low- and high-magnification images were obtained from an FSX100 microscope (Olympus).

Morphometry

A stereological point grid was superimposed on digital images of biotinylated isolectin $B4^+$ vessels using ImageJ software. The ratio between points falling on blood vessels and on brain tissue was calculated for each section, and average values were obtained.

Cell counting

Profiles of $GABA^+$ immunoreactive cells were counted in the prefrontal cortex (at bregma levels 1.5, 0.5, and −1.5) using stereotaxic coordinates from the atlas "The Mouse Brain in Stereotaxic Coordinates," by Paxinos and Franklin (*33*). For each area, cells in the strip of cortex from the pial surface to the white-gray matter interface were counted using ImageJ software and plotted. Details of sample size evaluation are provided in the "Statistical analysis" section, and sample sizes and brain region used for cell counting are provided in figure legends.

Primary culture of endothelial cells and endothelial cell stainings

Embryonic brains were dissected under a stereo microscope after the NAD^+ treatment paradigm, and the telencephalon was removed. Pial membranes were peeled off. Telencephalon without pial membranes from the periventricular region was pooled. Purity of endothelial cell cultures was established with endothelial cell markers and determined to be 100% (*4*, *12*). Isolation and culture of endothelial cells were performed according to published methodology (*4*, *12*). Periventricular endothelial cells were prepared from CD1 (wild type), saline-treated *Gabrb3*$^{fl/fl}$, saline-treated *Gabrb3*^{ECKO}, and NAD^+-treated *Gabrb3*^{ECKO} embryos. Endothelial cells were labeled with anti–biotinylated isolectin B4 (1:100, Sigma-Aldrich), anti-GABA (1:400, Sigma-Aldrich), anti-DAXX (1:100, Santa Cruz Biotechnology), and anti-P2X4 (1:100, ABclonal) followed by secondary detection with Alexa Fluor conjugates (Invitrogen). DAPI (Invitrogen) was used to label nuclei. Images were taken on an FSX100 microscope (Olympus). One million cells were examined for each IHC condition.

Endothelial cell proliferation and long-distance cell migration assay

To test for cell proliferation, CD1 periventricular endothelial cells (1 million cells per experiment) were incubated in the presence of the mitotic marker BrdU (0.05%) with or without muscimol for 1 hour to examine the impact on proliferation of these cells and processed for BrdU IHC (*1*, *4*).

In preparation for long-distance cell migration assays, square culture inserts (ibidi GmbH) were placed at one end of a 35-mm dish. Cultures of CD1-derived endothelial cells, purified from the periventricular plexus, were plated in the insert and allowed to migrate for 24 hours in endothelial cell culture medium. Endothelial cells were labeled with a cell trace marker (CellLight Plasma Membrane-RFP, BacMam 2.0, Invitrogen) to visualize endothelial cell morphologies during subsequent imaging. The migration of endothelial cells from one end of the dish to the other spanning a distance of 3.5 cm was imaged and quantified.

Isolation and primary culture of neuronal cells

Primary culture of embryonic GABAergic neurons from CD1 telencephalon or after the saline or NAD^+ treatment paradigms was performed using established methods (*5*). Briefly, embryonic brains were extracted under a stereo microscope and placed into cold phosphate-buffered saline (PBS). After removal of the pial membrane, the telencephalon was dissected from each embryonic brain. The telencephalon was minced into 1- to 2-mm slices in cold PBS. Minced telencephalon was treated with 0.1X trypsin/EDTA at 37°C for 5 min. Trypsin treatment was stopped by adding fetal bovine serum–Dulbecco's modified Eagle's medium and deoxyribonuclease I consecutively. Dissociated cells were filtered with a 40-μm cell strainer, and last, filtered cells were cultured in poly-D-lysine–coated culture dishes

with Neurobasal medium (Life Technologies) with 1× B-27 (Life Technologies) and 1× GlutaMAX (Life Technologies).

Neuronal migration assay

In preparation for cell migration assays, one-well square culture inserts (ibidi GmbH) were placed in the center of a poly-ornithine/laminin–coated 35-mm dish to make a small rectangular patch that is labeled outside the dish. Embryonic neurons prepared from the saline and NAD^+-treated groups were seeded in the inserts in Neurobasal medium supplemented with 1× B-27 and 1× GlutaMAX. After the cells had attached, the inserts were removed to initiate cell migration in all four quadrants of the dish. After 24 hours, cells were fixed and labeled with anti–β-tubulin antibody (1:2000, BioLegend). Neuronal migration was assessed by measuring the distance between the final positions of cells from the border of the rectangular patch outlined on the first day, using ImageJ software.

Calcium imaging

For Ca^{2+} assays, periventricular endothelial cells (1 million cells per assay) were incubated with the Ca^{2+} indicator dye FluoForte AM according to the manufacturer's instructions (Enzo Life Sciences), loaded into the chamber of an FSX100 microscope, and imaged continuously before and after αβ-meATP, Bz-ATP, and 2Me-SADP application (100 μM). Fluorescence micrographs were digitalized, and results were expressed as change in fluorescence over baseline fluorescence.

Gene expression profile analysis

RNA samples were prepared from saline-treated *Gabrb3*$^{fl/fl}$, saline-treated *Gabrb3*^{ECKO}, and NAD^+-treated *Gabrb3*^{ECKO} groups from three different brain pools. Total RNA from each of the samples was extracted by using the PicoPure RNA Isolation kit (Arcturus) following the supplier's protocol. Microarray was performed with the Mouse Gene 2.0 ST Array (Affymetrix) at the Boston University Microarray & Sequencing Resource, Boston, MA. Mouse Gene 2.0 ST CEL files were normalized to produce gene-level expression values using the implementation of the robust multiarray average (*34*) in the affy package (version 1.36.1) (*35*) included in the Bioconductor software suite (version 2.11) (*36*). PCA was analyzed and visualized using Transcriptome Analysis Console 4.0 (Affymetrix). Heatmap visualization and analysis were performed using Morpheus (Broad Institute, Boston, MA, USA; https://software.broadinstitute.org/GENE-E/) and ranked by *t* test statistics. Violin plot visualization was generated with *Z* score using GraphPad Prism v8.0 (GraphPad Software, La Jolla, CA, USA). The GO for gene enrichment study was performed in three GO TERM annotation categories by using the Database for Annotation, Visualization and Integrated Discovery v6.8. Mouse Genome Informatics (GO TERM structure categories: cerebral cortex interneuron migration, GABAergic neuron differentiation, interneuron development, and MGE-derived cells).

Quantitative real-time PCR

Reverse transcription was performed by using the iScript Reverse Transcription Supermix kit (Bio-Rad). PCRs were run on a CFX96 Touch Real-Time PCR (Bio-Rad) with SsoAdvanced Universal SYBR Green Supermix (Bio-Rad). Primers for qPCR (*Daxx*, *P2x4*, *P2x7*, *P2y13*, *Tek*, *vwf*, *F2r*, *Sirt2*, *Nos1*, *Nrp1*, *Pax6*, *Gad1*, *Gad2*, *Grin2a*, *Trpm2*, *Trpc4*, and *Trpv6*) were obtained from Thermo Fisher Scientific. The housekeeping gene *Gapdh* was used as a reference. The relative gene expression and subsequent fold changes among different samples were determined according to published methodology (*37*).

Enzyme-linked immunosorbent assay

Periventricular endothelial cells were prepared after the NAD^+ treatment paradigm, or after the treatment with purinergic receptor agonists/antagonists, and seeded in 12-well culture plates at 0.1×10^6 cells per well. Supernatants from endothelial cell cultures were collected after 96 hours and stored at −80°C for ELISA. GABA concentrations were quantitatively determined by competitive ELISA according to the manufacturers' protocol (GABA Research ELISA kits, Labor Diagnostica Nord, Germany), and absorbance was measured using a multiplate microplate fluorescence reader (Molecular Devices, CA) at 450 nm.

In vivo imaging of brain microvasculature by MPLSM

In vivo imaging of the brain vasculature in cranial window–bearing mice was performed as described previously (*26*, *27*). Briefly, a cranial window was implanted by removing a circular area of skull and dura. Then, the window was sealed with a 7-mm cover glass glued to the bone. For the measurement of RBC velocity and blood vessel diameter, we used MPLSM (*28*). To avoid potential tissue/vessel alteration caused by the window implantation procedure, we performed imaging at least 10 days after cranial window implantation. For imaging, mice were anesthetized with ketamine/xylazine, and then tetramethylrhodamine (TAMRA)–dextran (weight-average molecular weight, 500,000) was administrated through retro-orbital injection. Using TAMRA-dextran contrast-enhanced angiography, region of interest is first identified. Since the intravenously injected dye labels only the blood plasma, RBCs appear as dark patches moving within the vessel lumen. Centerline RBC velocity was measured by repetitively scanning a line along the central axis of a single blood vessel (*x*-*t*) and enabling the tracking of the motion of these dark patches. The space-time image produced by the line scan contained diagonal dark streaks formed by moving RBCs, with a slope that was inversely proportional to the centerline RBC velocity. This space-time image was then computationally processed using MATLAB and Python to extract the gradient of each streak, corresponding to the RBC velocity. Briefly, diagonal filters of varying gradients were tested for each streak until the gradient that fit best was found. This was conducted for each streak in the space-time image, and the mean gradient was taken. For the vessel diameter, an edge filter was applied to determine the blood vessel boundaries and the blood vessel diameter extracted at the indicated region of interest. The blood flow rate was determined through the following formula

$$\dot{Q} = \pi r^2 \dot{v}$$

where $\dot{Q}$ is the final flow rate, r is the vessel radius, and $\dot{v}$ is the blood flow velocity.

Behavioral experiments

Mice were housed in our animal facility with a 12-hour light cycle with ad libitum access to food and water. Offspring stayed with their mothers until weaning at postnatal day 21 after which males and females were separated. Before all behavioral testing, mice were acclimated to the testing room for 1 hour. Behavioral assays were performed according to established protocols referenced here:

self-grooming (*38*), light-dark box (*39*), tail suspension test (*40*), Y-maze (*39*), open-field locomotion activity (fig. S10), three-chamber social interaction test (*41*), and nest building with nestlets (*42*) and with shredded paper (*43*). Both males and females were used for all behavioral assays. Experimenters scoring behaviors were blinded to the genotypes and treatment. Sample sizes for each assay are noted in figure legends.

Statistical analysis

For each experiment, we used samples collected from either one or two embryos of the same genotype or postnatal mice from a given litter. We used 5 to 10 litters of mice for each prenatal experiment and 3 to 10 litters of mice for each postnatal experiment. Thus, we used data from 8 to 10 individuals per prenatal and postnatal condition. For behavioral experiments, 8 to 16 litters of mice were used. Statistical significance of differences between groups was analyzed by either one-way analysis of variance (ANOVA) or two-tailed Student's *t* test (GraphPad Prism software) and has been noted in individual figure legends. Significance was reported at $P < 0.05$.

SUPPLEMENTARY MATERIALS

Supplementary material for this article is available at http://advances.sciencemag.org/cgi/content/full/6/41/eabb9766/DC1

View/request a protocol for this paper from *Bio-protocol*.

REFERENCES AND NOTES

1. S. Li, P. Kumar T, S. Joshee, T. Kirschstein, S. Subburaju, J. S. Khalili, J. Kloepper, C. du, A. Elkhal, G. Szabó, R. K. Jain, R. Köhling, A. Vasudevan, Endothelial cell-derived GABA signaling modulates neuronal migration and postnatal behavior. *Cell Res.* **28**, 221–248 (2018).
2. C. Won, Z. Lin, P. Kumar T., S. Li, L. Ding, A. Elkhal, G. Szabó, A. Vasudevan, Autonomous vascular networks synchronize GABA neuron migration in the embryonic forebrain. *Nat. Commun.* **4**, 2149 (2013).
3. S. Li, K. Haigh, J. J. Haigh, A. Vasudevan, Endothelial VEGF sculpts cortical cytoarchitecture. *J. Neurosci.* **33**, 14809–14815 (2013).
4. A. Vasudevan, J. E. Long, J. E. Crandall, J. L. Rubenstein, P. G. Bhide, Compartment-specific transcription factors orchestrate angiogenesis gradients in the embryonic brain. *Nat. Neurosci.* **11**, 429–439 (2008).
5. Y. K. Choi, A. Vasudevan, Mechanistic insights into autocrine and paracrine roles of endothelial GABA signaling in the embryonic forebrain. *Sci. Rep.* **9**, 16256 (2019).
6. S. G. Tullius, H. R. C. Biefer, S. Li, A. J. Trachtenberg, K. Edtinger, M. Quante, F. Krenzien, H. Uehara, X. Yang, H. T. Kissick, W. P. Kuo, I. Ghiran, M. A. de la Fuente, M. S. Arredouani, V. Camacho, J. C. Tigges, V. Toxavidis, R. el Fatimy, B. D. Smith, A. Vasudevan, A. ElKhal, NAD^+ protects against EAE by regulating $CD4^+$ T-cell differentiation. *Nat. Commun.* **5**, 5101 (2014).
7. G. J. Burton, A. L. Fowden, The placenta: A multifaceted, transient organ. *Philos. Trans. R. Soc. Lond. B Biol. Sci.* **370**, 20140066 (2015).
8. M. Ushio-Fukai, Redox signaling in angiogenesis: Role of NADPH oxidase. *Cardiovasc. Res.* **71**, 226–235 (2006).
9. A. Das, G. X. Huang, M. S. Bonkowski, A. Longchamp, C. Li, M. B. Schultz, L. J. Kim, B. Osborne, S. Joshi, Y. Lu, J. H. Treviño-Villarreal, M. J. Kang, T. T. Hung, B. Lee, E. O. Williams, M. Igarashi, J. R. Mitchell, L. E. Wu, N. Turner, Z. Arany, L. Guarente, D. A. Sinclair, Impairment of an endothelial NAD^+-H_2S signaling network is a reversible cause of vascular aging. *Cell* **173**, 74–89.e20 (2018).
10. N. Braidy, R. Grant, P. S. Sachdev, Nicotinamide adenine dinucleotide and its related precursors for the treatment of Alzheimer's disease. *Curr. Opin. Psychiatry* **31**, 160–166 (2018).
11. P. H. Ear, A. Chadda, S. B. Gumusoglu, M. S. Schmidt, S. Vogeler, J. Malicoat, J. Kadel, M. M. Moore, M. E. Migaud, H. E. Stevens, C. Brenner, Maternal nicotinamide riboside enhances postpartum weight loss, juvenile offspring development, and neurogenesis of adult offspring. *Cell Rep.* **26**, 969–983.e4 (2019).
12. P. Kumar T, A. Vasudevan, Isolation and culture of endothelial cells from the embryonic forebrain. *J. Vis. Exp.* , e51021 (2014).
13. S. A. Anderson, O. Marin, C. Horn, K. Jennings, J. L. Rubenstein, Distinct cortical migrations from the medial and lateral ganglionic eminences. *Development* **128**, 353–363 (2001).
14. O. Marín, J. L. R. Rubenstein, A long, remarkable journey: Tangential migration in the telencephalon. *Nat. Rev. Neurosci.* **2**, 780–790 (2001).
15. J. G. Corbin, S. Nery, G. Fishell, Telencephalic cells take a tangent: Non-radial migration in the mammalian forebrain. *Nat. Neurosci.* **4**, 1177–1182 (2001).
16. L. Sussel, O. Marin, S. Kimura, J. L. Rubenstein, Loss of Nkx2.1 homeobox gene function results in a ventral to dorsal molecular respecification within the basal telencephalon: Evidence for a transformation of the pallidum into the striatum. *Development* **126**, 3359 (1999).
17. S. Nobrega-Pereira, N. Kessaris, T. Du, S. Kimura, S. A. Anderson, O. Marín, Postmitotic Nkx2-1 controls the migration of telencephalic interneurons by direct repression of guidance receptors. *Neuron* **59**, 733–745 (2008).
18. A. N. Rubin, N. Kessaris, PROX1: A lineage tracer for cortical interneurons originating in the lateral/caudal ganglionic eminence and preoptic area. *PLOS ONE* **8**, e77339 (2013).
19. S. Subburaju, A. J. Coleman, W. B. Ruzicka, F. M. Benes, Toward dissecting the etiology of schizophrenia: HDAC1 and DAXX regulate GAD67 expression in an in vitro hippocampal GABA neuron model. *Transl. Psychiatry* **6**, e723 (2016).
20. S. Subburaju, F. M. Benes, Induction of the GABA cell phenotype: An in vitro model for studying neurodevelopmental disorders. *PLOS ONE* **7**, e33352 (2012).
21. S. Subburaju, A. J. Coleman, M. G. Cunningham, W. B. Ruzicka, F. M. Benes, Epigenetic regulation of glutamic acid decarboxylase 67 in a hippocampal circuit. *Cereb. Cortex* **27**, 5284–5293 (2017).
22. D. F. Owens, A. R. Kriegstein, Patterns of intracellular calcium fluctuation in precursor cells of the neocortical ventricular zone. *J. Neurosci.* **18**, 5374–5388 (1998).
23. K. Yamamoto, T. Sokabe, T. Matsumoto, K. Yoshimura, M. Shibata, N. Ohura, T. Fukuda, T. Sato, K. Sekine, S. Kato, M. Isshiki, T. Fujita, M. Kobayashi, K. Kawamura, H. Masuda, A. Kamiya, J. Ando, Impaired flow-dependent control of vascular tone and remodeling in P2X4-deficient mice. *Nat. Med.* **12**, 133–137 (2006).
24. L. Stokes, J. A. Layhadi, L. Bibic, K. Dhuna, S. J. Fountain, P2X4 receptor function in the nervous system and current breakthroughs in pharmacology. *Front. Pharmacol.* **8**, 291 (2017).
25. K. A. Jacobson, P2X and P2Y Receptors (Tocris Bioscience Scientific Review **No. 33**, 2010).
26. R. K. Jain, L. L. Munn, D. Fukumura, Dissecting tumour pathophysiology using intravital microscopy. *Nat. Rev. Cancer* **2**, 266–276 (2002).
27. R. K. Jain, L. L. Munn, D. Fukumura, Measuring angiogenesis and hemodynamics in mice. *Cold Spring Harb. Protoc.* **2013**, 354–358 (2013).
28. E. B. Brown, R. B. Campbell, Y. Tsuzuki, L. Xu, P. Carmeliet, D. Fukumura, R. K. Jain, In vivo measurement of gene expression, angiogenesis and physiological function in tumors using multiphoton laser scanning microscopy. *Nat. Med.* **7**, 864–868 (2001).
29. A. Hoffer, H. Osmond, Nicotinamide adenine dinucleotide in the treatment of chronic schizophrenic patients. *Br. J. Psychiatry* **114**, 915–917 (1968).
30. N. S. Kline, G. L. Barclay, J. O. Cole, A. H. Esser, H. Lehmann, J. R. Wittenborn, Controlled evaluation of nicotinamide adenine dinucleotide in the treatment of chronic schizophrenic patients. *Br. J. Psychiatry* **113**, 731–742 (1967).
31. N. S. Kline, G. L. Barclay, A. H. Esser, J. O. Cole, H. E. Lehmann, J. R. Wittenborn, Diphosphopyridine nucleotide in the treatment of schizophrenia. *JAMA* **200**, 881–882 (1967).
32. S. Y. Kim, B. M. Cohen, X. Chen, S. E. Lukas, A. K. Shinn, A. C. Yuksel, T. Li, F. du, D. Öngür, Redox dysregulation in schizophrenia revealed by in vivo NAD^+/NADH Measurement. *Schizophr. Bull.* **43**, 197–204 (2017).
33. G. Paxinos, K. Franklin, *The Mouse Brain in Stereotaxic Coordinates*, 3rd edition (Academic Press, San Diego, 2007).
34. M. E. Ritchie, B. Phipson, D. Wu, Y. Hu, C. W. Law, W. Shi, G. K. Smyth, limma powers differential expression analyses for RNA-sequencing and microarray studies. *Nucleic Acids Res.* **43**, e47 (2015).
35. L. Gautier, L. Cope, B. M. Bolstad, R. A. Irizarry, affy--analysis of Affymetrix GeneChip data at the probe level. *Bioinformatics* **20**, 307–315 (2004).
36. R. C. Gentleman, V. J. Carey, D. M. Bates, B. Bolstad, M. Dettling, S. Dudoit, B. Ellis, L. Gautier, Y. Ge, J. Gentry, K. Hornik, T. Hothorn, W. Huber, S. Iacus, R. Irizarry, F. Leisch, C. Li, M. Maechler, A. J. Rossini, G. Sawitzki, C. Smith, G. Smyth, L. Tierney, J. Y. H. Yang, J. Zhang, Bioconductor: Open software development for computational biology and bioinformatics. *Genome Biol.* **5**, R80 (2004).
37. K. J. Livak, T. D. Schmittgen, Analysis of relative gene expression data using real-time quantitative PCR and the $2^{-\Delta\Delta C}_T$ method. *Methods* **25**, 402–408 (2001).
38. J. L. Silverman, S. S. Tolu, C. L. Barkan, J. N. Crawley, Repetitive self-grooming behavior in the BTBR mouse model of autism is blocked by the mGluR5 antagonist MPEP. *Neuropsychopharmacology* **35**, 976–989 (2010).
39. J. N. Crawley, *What's Wrong With My Mouse? Behavioral Phenotyping of Transgenic and Knockout mice* (Wiley, 2007).
40. A. Can, D. T. Dao, C. E. Terrillion, S. C. Piantadosi, S. Bhat, T. D. Gould, The tail suspension test. *J. Vis. Exp*, 3769 (2012).

41. M. J. Kane, M. Angoa-Peréz, D. I. Briggs, C. E. Sykes, D. M. Francescutti, D. R. Rosenberg, D. M. Kuhn, Mice genetically depleted of brain serotonin display social impairments, communication deficits and repetitive behaviors: Possible relevance to autism. *PLOS ONE* **7**, e48975 (2012).
42. R. M. J. Deacon, Assessing nest building in mice. *Nat. Protoc.* **1**, 1117–1119 (2006).S. E. Hess, S. Rohr, B. D. Dufour, B. N. Gaskill, E. A. Pajor, J. P. Garner, Home improvement: C57BL/6J mice given more naturalistic nesting materials build better nests. *J. Am. Assoc. Lab. Anim. Sci.* **47**, 25–31 (2008).
43. S. E. Hess, S. Rohr, B. D. Dufour, B. N. Gaskill, E. A. Pajor, J. P. Garner, Home improvement: C57BL/6J mice given more naturalistic nesting materials build better nests. *J. Am. Assoc. Lab. Anim. Sci.* **47**, 25–31 (2008).

Acknowledgments

Funding: This work was supported by awards from the National Institute of Mental Health (R01MH110438) and National Institute of Neurological Disorders and Stroke (R01NS100808) to A.V. The MGH team and the blood flow contributions, in part, were supported by R01CA208205, R35CA197743, and U01CA224173 from the National Cancer Institute and Harvard Ludwig Cancer Center to D.F. and R.K.J. J.R. was supported by an award from the Cancer Research Institute and is a Dr. Keith Landesman Memorial fellow. A.S.K. was supported by an A*STAR NSS (PhD) graduate scholarship. **Author contributions:** A.V. conceived and designed the project. S.S. performed NAD^+ administration, brain isolations, brain tissue processing, cryosections preparation, IHC, gene expression profile analysis, qRT-PCR, and calcium imaging. S.S. and S.K. performed mouse colony maintenance, genotyping, histology, and behavioral assays. J.B. performed IHC and imaging. Y.K.C. performed endothelial and neuronal cell culture, calcium imaging, and behavioral assays. D.D. performed cell migration assays and immunocytochemistry. J.R., A.S.K., D.F., and R.K.J. (MGH research team) designed the blood vessel function studies and assessed microvascular blood flow using a cranial window model and intravital multiphoton microscopy; J.R. and A.S.K. performed experiments, and J.R., A.S.K., D.F., and R.K.J. analyzed, interpreted, and wrote the blood flow results and method sections. G.S. provided the GAD65-GFP line. A.E. contributed the ELISA results and expertise with NAD^+ administration. S.S. and A.V. analyzed data, prepared figures, and wrote the manuscript. J.R., G.S., D.F., R.K.J., and A.E. provided comments on the manuscript. A.V. supervised and coordinated all aspects of the project. **Competing interests:** A.V. is an inventor on a provisional patent related to this work (Filing date: 09/28/20 and provisional application number: 63084230). We disclose that R.K.J. received honorarium from Amgen and consultant fees from Chugai, Ophthotech, Merck, Pfizer, and SPARC. R.K.J. owns equity in Enlight, Ophthotech, and SynDevRx and serves on the Scientific Advisory Board of Accurius Therapeutics and the Boards of Trustees of Tekla Healthcare Investors, Tekla Life Sciences Investors, Tekla Healthcare Opportunities Fund, and Tekla World Healthcare Fund. We also disclose that D.F. received consultant fee from Merck. No funding or reagents from these companies were used in this study. The other authors declare that they have no competing interests. **Data and materials availability:** All data needed to evaluate the conclusions in the paper are present in the paper and/or the Supplementary Materials. Additional data related to this paper may be requested from the authors.

Submitted 30 March 2020
Accepted 26 August 2020
Published 9 October 2020
10.1126/sciadv.abb9766

Citation: S. Subburaju, S. Kaye, Y. K. Choi, J. Baruah, D. Datta, J. Ren, A. S. Kumar, G. Szabo, D. Fukumura, R. K. Jain, A. Elkhal, A. Vasudevan, NAD^+-mediated rescue of prenatal forebrain angiogenesis restores postnatal behavior. *Sci. Adv.* **6**, eabb9766 (2020).